Mathematical Modelling in Foam Dynamics via Domain Decomposition

Stefan Petrevski

Christ Church

University of Oxford

BEE Extended Essay submitted towards

FHS Mathematics (Part B)

Hilary Term, 2020

Acknowledgements

First and foremost, I would like to thank my official supervisor, Prof. Chris Breward, who kindly introduced me to the topic of his dissertation as a gateway for my first insight into applied mathematics research. During the supervision meetings, he ensured that I properly understood underlying core physical concepts before working on the underlying mathematics. Moreover, I should like to thank Prof. Peter Howell for the kind conversation we had on research he conducted over two decades ago. His suggestions steered me in the direction towards the surface viscosity extensions in the final chapter. Finally, I would like to express gratitude to Arkady Wey of the InFoMM CDT at Oxford, who gave me an informal tutorial on using Inkscape to produce diagrams in conjunction with LaTeX.

Abstract

We study mathematical models of liquid foam stability through the work of Breward & Howell [7], synthesising it with later generalisations due to Brush & Davis [8]. In later chapters, we examine the effects of flow retardation as caused by the presence of surfactants, by initially considering an early model of Schwartz & Princen [20]. Subsequently, we conduct a sophisticated and exhaustive study of surfactants through surface viscosity as studied by Breward [5], ultimately discovering how this phenomenon behaves within the generalised configuration of Brush & Davis. Lastly, we introduce a new regime of low surface viscosity, which we intepret through numerical solutions of the resulting differential equations.

Contents

List of Figures

Chapter 1

Introduction

1.1 Why study foams?

Liquid foams have overarching industrial applications ranging from crop spraying to explosion dampening. A primary reason for the significance of foams is the ability to distribute small portions of liquid over an extensive area, which is in turn crucial in maximisation endeavours under a constraint on the liquid matter.

On the other hand, presence of foams in different circumstances may be undesirable. For instance, a frequent issue at gas stations is the formation of foam films in car tanks, whereby the tank's volume is prematurely occupied by foam instead of fuel [19]. Similarly, the creation of foam in beer production not only limits the storing capacity, but also diminishes the "foaminess" of servings [5].

For such reasons, it is important to understand both the macroscopic behaviour of foams themselves, as well as their dependence on key parameters and constituents. In this essay, we deal with the question of foam stability by considering models which yield laws of thinning and approximate lifetimes of unstable foams.

1.2 Properties of foam

1.2.1 Basic definitions

Firstly, we distinguish between **solid** and **liquid foams**. The former are crucial in creating stable, light materials (eg. aluminium foams), whereas the latter span industrial applications as described above. By definition, liquid foams are gas-liquid mixtures in which the portion of liquid volume is $\phi < 0.2$ (*cf.* *emulsions* whereby

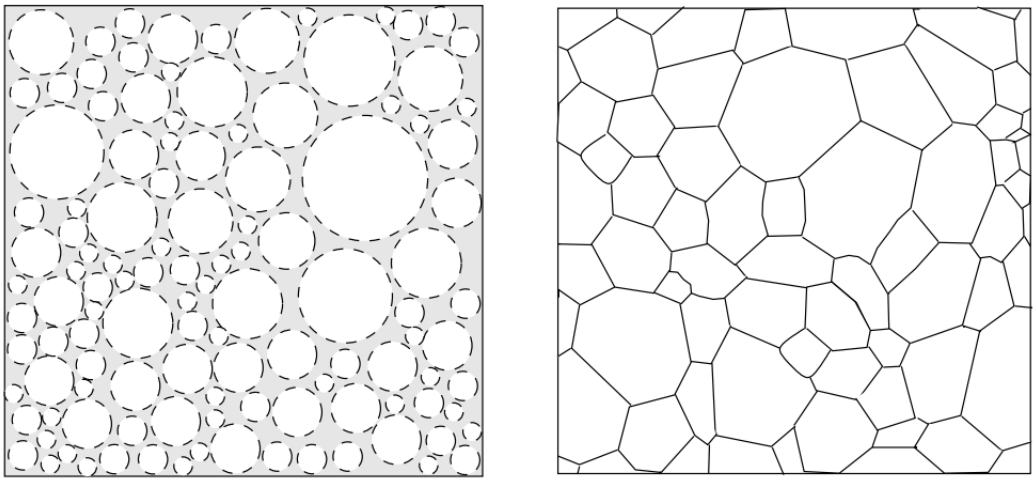

Figure 1.1: Schematic for wet foams with spherical bubbles (left) and dry foams with polygonal bubbles (right). Figure due to Breward [5].

$\phi \approx 0.9$). We may further sub-categorise liquid foams as **wet** ($0.1 < \phi < 0.2$) or **dry** ($\phi < 0.1$). Figure 1.1 shows the macroscopic differences. This is not an arbitrary convention: wet foams are characterised by spherical bubbles, whereas polyhedral bubbles are typical for dry foams. In this essay, we exclusively consider dry foams.

1.2.2 Components of liquid foams

We first classify constituents of liquid foams - their geometry and properties will be introduced in subsequent sections.

- **Lamellae (L)**: thin (and relatively flat) high-pressure liquid films forming polygonal faces.
- **Plateau Borders (PB)**: thick tubes of low-pressure liquid at the edges of the polyhedra, forming the bubbles of the foam.
- **Nodes (N)**: vertices of bubbles, junctions of Plateau borders.

1.3 Physical properties of films and foams

Previous studies on liquid foams have yielded both experimental and theoretical results. There are two main results that govern the dynamics of foam bubbles.

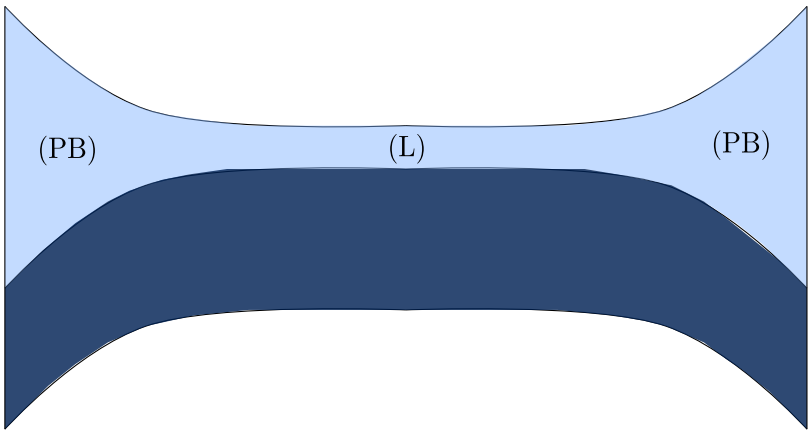

Figure 1.2: Top view: thickness varies from (L) to (PB).

1.3.1 Plateau's laws

Formulated in the 1870s by physicist Joseph Plateau, the laws read (see [23]):

(P1) Soap films are consisted of smooth, continuous surfaces.

(P2) The mean curvature of an element at a fixed point is always constant.

(P3) Three **lamellae** meet at a **Plateau border**, at an angle of $\pi/3$.

(P4) Four **Plateau borders** meet at a **node**, at an angle of $arccos(-\frac{1}{3}) \approx 109.47°$.

(P1)-**(P4)** are illustrated in Figure 1.3. The mathematical justification for these results is far from trivial. Namely, the first proof utilised geometric measure theory and was published by Taylor [21], some 200 years after Plateau's initial discovery.

1.3.2 Young-Laplace equation

Let ΔP be the pressure difference across a gas-liquid interface, σ be surface tension and R be the radius of curvature. Then, in a 2D geometry the following holds [23]:

$$\Delta p = \frac{2\sigma}{R}. \tag{1.1}$$

For foams, the significance is that any pressure difference arising between two phases forces the film separating them to exhibit curvature.

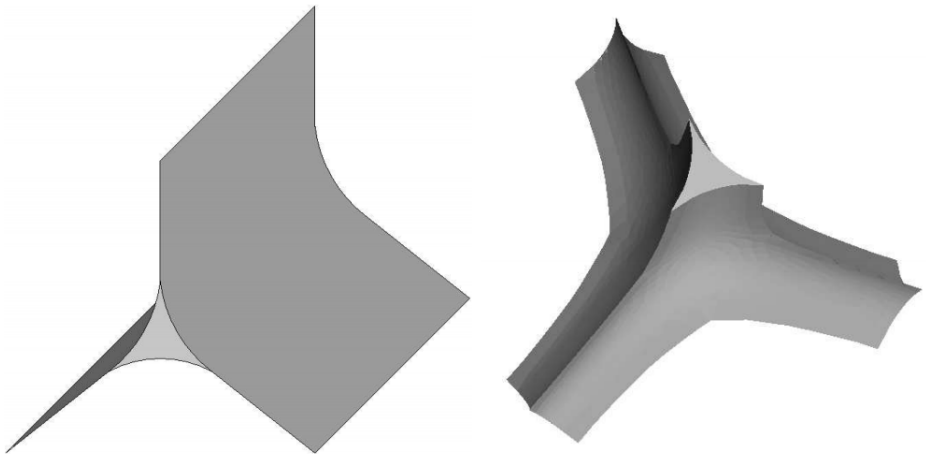

Figure 1.3: Geometry of **(P3)** (left) and **(P4)** (right). Figure by Schick [19].

1.4 Lamella vs. Plateau border drainage

The label "foam drainage" may be misleading, as two separate effects may fall under this description. Firstly, an existing foam is not necessarily in equilibrium: gravity will drive the flow of liquid located in (PB) regions. Under a set of assumptions, a second-order nonlinear PDE may be obtained:

$$\frac{\partial \alpha}{\partial \tau} + \frac{\partial}{\partial \xi}\left(\alpha^2 - \frac{\sqrt{\alpha}}{2}\frac{\partial \alpha}{\partial \xi}\right) = 0, \tag{1.2}$$

where α, τ, ξ represent non-dimensional cross-sectional area, time and vertical distance, respectively. This expression is a continuity equation for the flow rate through (PB). Its derivation assumes Plateau borders to be triangular regions, idealised as vertical channels and treated as a network. A linear stability analysis may be found in Verbist et al. [22], whereas a derivation is outlined in Weaire & Hutzler [23].

Many works only consider "foam drainage" as described above, neglecting contributions from lamellae. This may seem reasonable at the outset, as quantity of liquid in (PB) regions is typically orders of magnitude larger than in (L) regions. However, as presented in Chapter 4, this fails to be true for certain kinds of very dry liquid films. In addition, this treatment fails to consider aspects of foam stability. As illustrated in Figures 1.2 and 1.3, gas-liquid interfaces are curved, with pressure being lower in (PB) than in (L) regions. This pressure gradient drives a flux from (L) to (PB), which, if unopposed, leads to (L) eventually rupturing. There are means to counteract this and thereby extend the foam's lifetime: the most significant are **surfactants**, whose

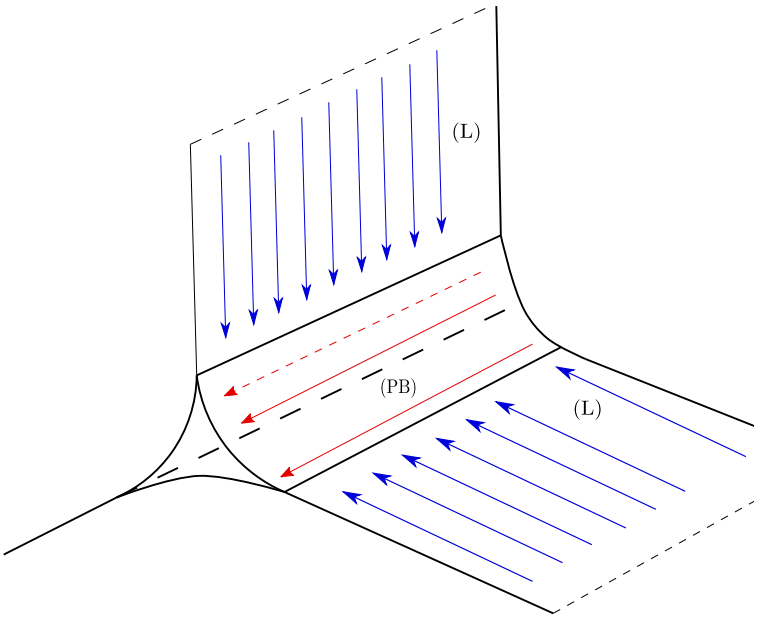

Figure 1.4: Gravity-driven (PB) drainage and pressure-driven (L) drainage.

molecules tend to reside at the interfaces and oppose flux by causing surface tension gradients.

Figure 1.4 illustrates this discussion. In this essay, we ignore the effects of gravity and focus solely on the rupture of thin lamellae due to the pressure-driven flux.

1.5 Overview of discussion

Chapter 2 provides a bottom-up derivation of governing equations for foam films. These PDEs form a starting point for a model by Breward & Howell [7], which introduces a transition region to reconcile solutions from (L) and (PB). There are numerous reasons for restricting attention to this work. While significant research was previously conducted by Barigou & Davidson [3] and Schwartz & Princen [20], their models include two more fictional regions in addition to (L) and (PB), as opposed to a single transition region that efficiently solves the model. Furthermore, Schwartz & Princen make extra assumptions on surfactant distributions, which precludes their separate, careful treatment. In contrast, Breward & Howell's model first builds a theory for surfactant-free foams, which can then admit sophisticated models for surfactants.

In Chapter 4, we highlight a work of Brush & Davis [8], which shows that for certain configurations, one of Breward & Howell's main assumptions breaks down. We then

carefully synthesise both approaches and resulting behaviours are directly compared. Next, Chapter 5 introduces Schwartz & Princen's simple approach to modelling surfactants as a gateway to more sophisticated treatments in Chapter 6, which focuses entirely on modelling surfactants via a constitutive relation on surface viscosity.

Original material can be found throughout the essay, including, but not limited, to the Plateau border argumentation of Section 3.1.2 and the classification of the (L) model in Section 3.2. The Lagrangian description in Chapter 6 and the introduction of surface viscosity in Brush & Davis' model are also original. Additionally, the low surface viscosity regime is new, while the linear stability analysis is similar to work by Breward [5] on Marangoni models, but involves new calculations.

The essay assumes familiarity with fluid dynamics, which can be obtained by reading Ockendon & Ockendon [16]. Facility with (partial) differential equations is more essential: understanding arguments requires working knowledge of A6: Differential Equations and B5.2: Applied PDEs.

Chapter 2

Derivation of Thin-Film Equations (TFEs)

2.1 Configuration and notation

To analyse foam lamellae, we consider thin-films whose surfaces form free liquid-air interfaces. We work in 2D, neglecting flow in/out of the $(x^\star, z^\star)$-plane, due to the (L)-(PB) geometry as in Figure 1.4. We modify and combine derivation procedures from [5] and [6], using the following notation:

- $h^\star(x^\star, t^\star)$ - film thickness.
- $\mathbf{u}^\star = (u^\star, w^\star)$ - liquid velocity in the $(x^\star, z^\star)$-plane.
- $p^\star$, $\mu^\star$, $\rho^\star$ - liquid pressure, viscosity, and density.
- $\sigma_\pm^\star$ - surface tension on top $(+)$ and bottom $(-)$ surfaces.
- L_0 - typical thin-film lengthscale.
- $\epsilon = \dfrac{\text{[typical thickness]}}{\text{[typical lengthscale]}} = \dfrac{h_0}{L_0} << 1.$
- $P_\pm^\star$ - constant atmospheric pressure above/below the thin-film.

We include a fictional centreline $H^\star(x^\star, t^\star)$, so the two free surfaces are given as in Figure 2.1:

$$z^\star - f_\pm^\star(x^\star, t^\star) = z^\star - \left(H^\star(x^\star, t^\star) \pm \frac{1}{2}h^\star(x^\star, t^\star)\right) = 0. \tag{2.1}$$

We use notation such as u_x and $\frac{\partial u}{\partial x}$ interchangeably to denote differentiation. Dimensional variables feature $\star$ superscripts, while lengthscales have 0 subscripts.

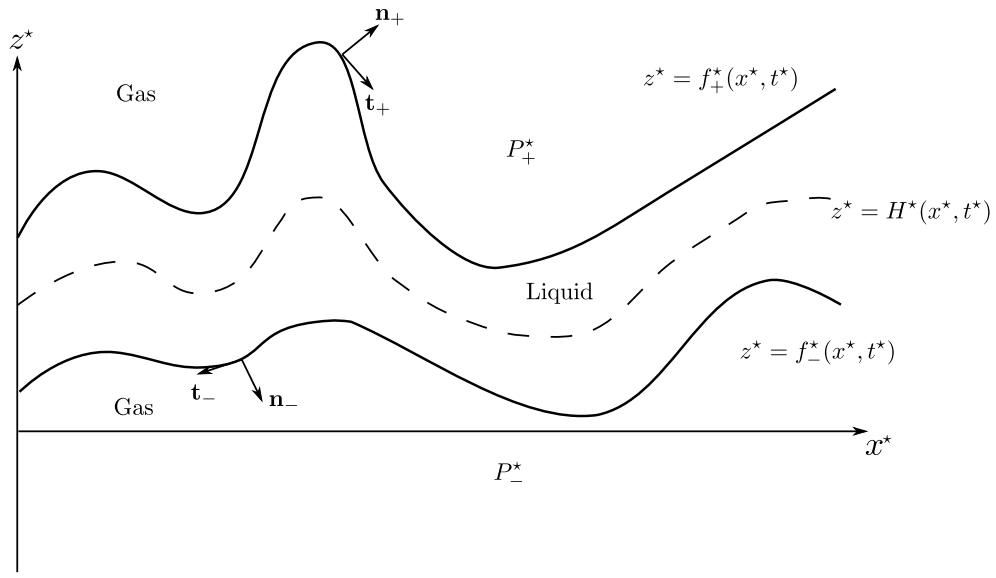

Figure 2.1: Free surfaces and their centreline.

2.2 Modelling assumptions

We assume that the viscous liquid obeys the continuum hypothesis of most practical flows, and that it has constant density. The governing equations are (see [16]):

Incompressible Navier-Stokes

$$\nabla \cdot \mathbf{u}^\star = 0, \tag{NS1*}$$

$$\rho^\star \frac{D\mathbf{u}^\star}{Dt^\star} = \rho^\star \left(\frac{\partial \mathbf{u}^\star}{\partial t^\star} + (\mathbf{u}^\star \cdot \nabla)\mathbf{u}^\star \right) = -\nabla p^\star + \mu^\star \nabla^2 \mathbf{u}^\star + \mathbf{F}^\star, \tag{NS2*}$$

where $D/Dt^\star$ is the convective derivative. Moreover, we assume absence of external forces, so $\mathbf{F}^\star = \mathbf{0}$. Equations (NS1*) and (NS2*) represent conservation of mass and momentum, respectively.

To analyse the boundaries, we must introduce stress components $\sigma_{ij}^\star$, representing force/unit area pointing along x_i, acting on elements with normal in the x_j direction. Viscous fluids have isotropic and deviatoric components, so their surfaces are described by the stress tensor τ (see [16]):

$$\tau = \begin{pmatrix} \sigma^\star_{11} & \sigma^\star_{13} \\ \sigma^\star_{31} & \sigma^\star_{33} \end{pmatrix} = \begin{pmatrix} -p^\star + 2\mu^\star \dfrac{\partial u^\star}{\partial x^\star} & \mu^\star \left(\dfrac{\partial u^\star}{\partial z^\star} + \dfrac{\partial w^\star}{\partial x^\star} \right) \\ \mu^\star \left(\dfrac{\partial u^\star}{\partial z^\star} + \dfrac{\partial w^\star}{\partial x^\star} \right) & -p^\star + 2\mu^\star \dfrac{\partial w^\star}{\partial z^\star} \end{pmatrix}. \tag{2.2}$$

Initially, we assume surfactants are absent, meaning no surface tension gradients occur at the boundaries $z^\star = f^\star_\pm(x^\star, t^\star)$. In fact, we set $\sigma^\star = \sigma^\star_+ = \sigma^\star_-$, given no volatile components alter the interfaces' material properties.

2.3 Boundary conditions

The total stress at a boundary is given by $\tau \mathbf{n}$, where $\mathbf{n}$ is the outward pointing unit normal. At $z^\star = f^\star_\pm(x^\star, t^\star)$, letting $\mathbf{t}_\pm$ be unit tangents corresponding to $\mathbf{n}_\pm$, we find:

$$\mathbf{n}_\pm = \pm \nabla F^\star_\pm(x^\star, t^\star) = \pm \frac{1}{\sqrt{1 + (H^\star_{x^\star} \pm \frac{1}{2} h^\star_{x^\star})^2}} \begin{pmatrix} -H^\star_{x^\star} \mp \frac{1}{2} h^\star_{x^\star} \\ 1 \end{pmatrix}, \tag{2.3}$$

$$\mathbf{t}_\pm = \pm \frac{1}{\sqrt{1 + (H^\star_{x^\star} \pm \frac{1}{2} h^\star_{x^\star})^2}} \begin{pmatrix} 1 \\ H^\star_{x^\star} \pm \frac{1}{2} h^\star_{x^\star} \end{pmatrix}. \tag{2.4}$$

The normal stress depends on curvature and pressure, while constant $\sigma^\star$ gives no shear stress, hence (see [12]):

Normal and tangential stress balances

$$\mathbf{n}_\pm \tau \mathbf{n}_\pm = P^\star_\pm \pm \sigma^\star_\pm \kappa^\star_\pm, \tag{2.5}$$

$$\mathbf{t}_\pm \tau \mathbf{n}_\pm = 0, \tag{2.6}$$

where $\kappa^\star_\pm$ represents mean curvature at $z^\star = f^\star_\pm(x^\star, t^\star)$:

$$\kappa^\star = \frac{f^\star_{x^\star x^\star}}{(1 + f^{\star 2}_{x^\star})^{\frac{3}{2}}}. \tag{2.7}$$

Evaluating (2.5)-(2.6) on $z^\star = f^\star_\pm(x^\star, t^\star)$, we get:

$$\pm \sigma_\pm \kappa_\pm = P^\star_\pm - p^\star + 2\mu^\star \frac{\left(u^\star_{x^\star} (H^\star_{x^\star} \pm \frac{1}{2} h^\star_{x^\star})^2 - (H^\star_{x^\star} \pm \frac{1}{2} h^\star_{x^\star}) w^\star_{x^\star} - u^\star_{z^\star} (H^\star_{x^\star} \pm \frac{1}{2} h^\star_{x^\star}) + w^\star_{z^\star} \right)}{1 + (H^\star_{x^\star} \pm \frac{1}{2} h_{x^\star})^2}, \tag{BC1*}$$

$$(u^\star_{z^\star} + w^\star_{x^\star}) \left(1 - (H^\star_{x^\star} \pm \frac{1}{2} h_{x^\star})^2 \right) + 2 (H^\star_{x^\star} \pm \frac{1}{2} h^\star_{x^\star})(w^\star_{z^\star} - u^\star_{x^\star}) = 0. \tag{BC2*}$$

The final boundary phenomenon is the *kinematic condition*, which ensures that particles residing on $F^\star_\pm(x^\star, t^\star) = 0$ remain there at all times, so (2.1) is always obeyed:

$$\frac{DF_\pm}{Dt^\star} = \frac{D}{Dt^\star}\left(z^\star - H^\star(x^\star, t^\star) \mp \frac{1}{2}h^\star(x^\star, t^\star)\right) = 0. \tag{2.8}$$

This leaves us with:

Kinematic condition

$$w^\star = H^\star_{t^\star} \pm \frac{1}{2}h^\star_{t^\star} + u^\star\left(H^\star_{x^\star} \pm \frac{1}{2}h^\star_{x^\star}\right) \text{ on } z^\star = f^\star_\pm(x^\star, t^\star) \tag{BC3*}$$

2.4 Nondimensionalisation

With U_0, P_0 unknown at present, we nondimensionalise:

Lubrication scalings

$$\begin{aligned} x^\star &= L_0 x, & z^\star &= \epsilon L_0 z, \\ u^\star &= U_0 u, & w^\star &= \epsilon U_0 w, \\ p^\star &= P_0 p, & t^\star &= \tfrac{L_0}{U_0} t, \\ H^\star \pm \tfrac{1}{2}h^\star &= \epsilon L_0(H \pm \tfrac{1}{2}h). \end{aligned} \tag{2.9}$$

Substituting (2.9) into the component form of (NS1*)-(NS2*) and defining the *Reynolds number* $\mathrm{Re} = \rho^\star U_0 L_0/\mu^\star$, we see:

$$\frac{\partial u}{\partial x} + \frac{\partial w}{\partial z} = 0, \tag{NS1}$$

$$\epsilon^2 \mathrm{Re}\frac{Du}{Dt} = -\epsilon^2\left[\frac{P_0 L_0}{\mu^\star U_0}\right]\frac{\partial p}{\partial x} + \epsilon^2\frac{\partial^2 u}{\partial x^2} + \frac{\partial^2 u}{\partial z^2}, \tag{2.10}$$

$$\epsilon^2 \mathrm{Re}\frac{Dw}{Dt} = -\left[\frac{P_0 L_0}{\mu U_0}\right]\frac{\partial p}{\partial z} + \epsilon^2\frac{\partial^2 w}{\partial x^2} + \frac{\partial^2 w}{\partial z^2}. \tag{2.11}$$

The physical significance of Re comes from:

$$\mathrm{Re} = \frac{\rho^\star U_0^2/L_0}{\mu^\star U_0/L_0^2} = \frac{[\text{inertia term in (NS2*)}]}{[\text{viscous term in (NS2*)}]}. \tag{2.12}$$

In most thin-film literature, inertia effects are negligible compared to viscosity, so $\mathrm{Re} << 1$. To balance viscous and pressure terms in (2.10) and (2.11), the bracketed pressure coefficient needs to be $O(1)$. We therefore set:

$$P_0 = \frac{\mu^\star U_0}{L_0}. \tag{2.13}$$

Then, (2.10)-(2.11) become:

$$\epsilon^2 \mathrm{Re}\frac{Du}{Dt} = -\epsilon^2\frac{\partial p}{\partial x} + \epsilon^2\frac{\partial^2 u}{\partial x^2} + \frac{\partial^2 u}{\partial z^2}, \tag{NS2x}$$

$$\epsilon^2 \mathrm{Re}\frac{Dw}{Dt} = -\frac{\partial p}{\partial z} + \epsilon^2\frac{\partial^2 w}{\partial x^2} + \frac{\partial^2 w}{\partial z^2}. \tag{NS2z}$$

Next, applying (2.9) to (BC1*), (BC2*), (BC3*), the conditions on $z^\star = f_\pm^\star(x^\star, t^\star)$ become:

$$\begin{aligned} \pm\frac{\epsilon}{\mathrm{Ca}}\frac{H_{xx} \pm \frac{1}{2}h_{xx}}{\left(1+\epsilon^2(H_x \pm \frac{1}{2}h_x)^2\right)^{\frac{3}{2}}} = \\ P_\pm - p + 2\frac{\epsilon^2 u_x(H_x \pm \frac{1}{2}h_x)^2 - \epsilon^2(H_x \pm \frac{1}{2}h_x)w_x - u_z(H_x \pm \frac{1}{2}h_x) + w_z}{1+\epsilon^2(H_x \pm \frac{1}{2}h_x)^2} \end{aligned}, \tag{BC1}$$

$$(u_z + \epsilon^2 w_x)\left(1 - \epsilon^2(H_x \pm \frac{1}{2}h_x)^2\right) + 2\epsilon^2(H_x \pm \frac{1}{2}h_x)(w_z - u_x) = 0, \tag{BC2}$$

$$w = H_t \pm \frac{1}{2}h_t + u(H_x \pm \frac{1}{2}h_x). \tag{BC3}$$

The *capillary number* $\mathrm{Ca} = \mu^\star U_0/\sigma^\star$ in (BC1) represents the strength of capillary effects, measuring viscous drag versus surface tension. We consider configurations where $\epsilon/\mathrm{Ca} \sim O(1)$ or less (see Appendix A).

2.5 Asympotic analysis

Due to $\epsilon << 1$ in (NS2x) and (NS2z), we apply the following ansatz as $\epsilon \to 0^+$:

$$u(x,z,t) \sim u_0(x,z,t) + \epsilon^2 u_1(x,z,t) + o(\epsilon^2), \tag{2.14}$$

$$w(x,z,t) \sim w_0(x,z,t) + \epsilon^2 w_1(x,z,t) + o(\epsilon^2), \tag{2.15}$$

$$p(x,z,t) \sim p_0(x,z,t) + \epsilon^2 p_1(x,z,t) + o(\epsilon^2), \tag{2.16}$$

$$H(x,t) \sim H_0(x,t) + \epsilon^2 H_1(x,t) + o(\epsilon^2), \tag{2.17}$$

$$h(x,t) \sim h_0(x,t) + \epsilon^2 h_1(x,t) + o(\epsilon^2). \tag{2.18}$$

2.5.1 Equations at $O(1)$

Via (2.14)-(2.18), at $O(1)$ in ϵ, (NS1), (NS2x), and (NS2z) become:

Governing equations $O(1)$

$$\frac{\partial u_0}{\partial x} + \frac{\partial w_0}{\partial z} = 0, \tag{NS1$O(1)$}$$

$$\frac{\partial^2 u_0}{\partial z^2} = 0, \tag{NS2$xO(1)$}$$

$$\frac{\partial^2 w_0}{\partial z^2} - \frac{\partial p_0}{\partial z} = 0. \tag{NS2$zO(1)$}$$

Moreover, (BC1)-(BC3) at $z = H_0 \pm \frac{1}{2}h_0$ become:

$$\frac{\epsilon}{\mathrm{Ca}}\left(\pm \frac{\partial^2 H_0}{\partial x^2} + \frac{1}{2}\frac{\partial^2 h_0}{\partial x^2} \right) = P_\pm - p_0 + 2\frac{\partial w_0}{\partial z}, \tag{BC1$O(1)$}$$

$$\frac{\partial u_0}{\partial z} = 0, \tag{BC2$O(1)$}$$

$$w_0 = \frac{\partial H_0}{\partial t} \pm \frac{1}{2}\frac{\partial h_0}{\partial t} + u_0\left(\frac{\partial H_0}{\partial x} \pm \frac{1}{2}\frac{\partial h_0}{\partial x} \right). \tag{BC3$O(1)$}$$

2.5.2 Equations at $O(\epsilon^2)$

(NS1$O(1)$)-(NS2$zO(1)$) subject to (BC1$O(1)$)-(BC3$O(1)$) will be insufficient to solve (NS1)-(NS2z) at leading order. We therefore deduce (NS1)-(NS2z) at the next lowest order:

Governing equations $O(\epsilon^2)$

$$\frac{\partial u_1}{\partial x} + \frac{\partial w_1}{\partial z} = 0, \tag{NS1$O(\epsilon^2)$}$$

$$0 = -\frac{\partial p_0}{\partial x} + \frac{\partial^2 u_0}{\partial x^2} + \frac{\partial^2 u_1}{\partial z^2}, \tag{NS2$xO(\epsilon^2)$}$$

$$0 = -\frac{\partial p_1}{\partial y} + \frac{\partial^2 w_0}{\partial x^2} + \frac{\partial^2 w_1}{\partial z^2}. \tag{NS2$zO(\epsilon^2)$}$$

Analogously, we may find (BC1)-(BC3) at $O(\epsilon^2)$, but none will be necessary, other than tangential stress at $z = H_0 \pm \frac{1}{2}h_0$:

$$0 = \frac{\partial u_1}{\partial z} + \frac{\partial w_0}{\partial x} \pm \frac{\partial h_0}{\partial x}\left(\frac{\partial w_0}{\partial z} - \frac{\partial u_0}{\partial x} \right) = \frac{\partial u_1}{\partial z} + \frac{\partial w_0}{\partial x} \mp 2\frac{\partial h_0}{\partial x}\frac{\partial u_0}{\partial x} \tag{BC2$O(\epsilon^2)$}$$

2.6 Reduction to thin-film equations

We integrate the simplest equation (NS2$xO(1)$) twice and use (BC2$O(1)$) to find:

$$u_0 = u_0(x,t). \tag{2.19}$$

Therefore, the longitudinal velocity is uniform across the film. This insight enables us to integrate incompressibility (NS1$O(1)$):

$$w_0 = -z\frac{\partial u_0}{\partial x} + C(x,t). \tag{2.20}$$

We recall that (BC3$O(1)$) gives w_0 explicitly at $z = H_0 \pm \frac{1}{2}h_0$; substituting (2.20) into these conditions, we obtain:

$$-\left(H_0 + \frac{1}{2}h_0\right)\frac{\partial u_0}{\partial x} + C(x,t) = \frac{\partial H_0}{\partial t} + \frac{1}{2}\frac{\partial h_0}{\partial t} + u_0\left(\frac{\partial H_0}{\partial x} + \frac{1}{2}\frac{\partial h_0}{\partial x}\right), \tag{2.21}$$

$$-\left(H_0 - \frac{1}{2}h_0\right)\frac{\partial u_0}{\partial x} + C(x,t) = \frac{\partial H_0}{\partial t} - \frac{1}{2}\frac{\partial h_0}{\partial t} + u_0\left(\frac{\partial H_0}{\partial x} - \frac{1}{2}\frac{\partial h_0}{\partial x}\right). \tag{2.22}$$

Subtracting (2.21) from (2.22) yields a continuity equation:

Conservation of mass

$$\frac{\partial h_0}{\partial t} + \frac{\partial}{\partial x}\left(u_0 h_0\right) = 0. \tag{2.23}$$

Meanwhile, adding (2.21) and (2.22) determines $C(x,t)$:

$$C(x,t) = \frac{\partial H_0}{\partial t} + u_0\frac{\partial H_0}{\partial x} + H_0\frac{\partial u_0}{\partial x}, \tag{2.24}$$

which then gives w_0 via (2.20):

$$w_0 = \frac{\partial H_0}{\partial t} + \frac{\partial}{\partial x}\left(u_0 H_0\right) - z\frac{\partial u_0}{\partial x}. \tag{2.25}$$

In turn, (2.25) simplifies (NS2$zO(1)$) to give a vertically-uniform pressure:

$$p_0 = p_0(x,t). \tag{2.26}$$

Our progress with w_0 and p_0 becomes particularly useful with (BC1$O(1)$). As w_{0_z} and p_0 are z-independent, each surface gives equations with dependence solely on x and t:

$$\frac{\epsilon}{\mathrm{Ca}}\left(\frac{\partial^2 H_0}{\partial x^2} + \frac{1}{2}\frac{\partial^2 h_0}{\partial x^2}\right) = P_+ - p_0 - 2\frac{\partial w_0}{\partial z} \text{ on } z = H_0 + \frac{1}{2}h_0, \tag{2.27}$$

$$\frac{\epsilon}{\mathrm{Ca}}\left(-\frac{\partial^2 H_0}{\partial x^2}+\frac{1}{2}\frac{\partial^2 h_0}{\partial x^2}\right)=P_- - p_0 - 2\frac{\partial w_0}{\partial z} \text{ on } z=H_0-\frac{1}{2}h_0. \tag{2.28}$$

Subtracting (2.28) from (2.27) gives:

$$\frac{\partial^2 H_0}{\partial x^2}=\frac{\mathrm{Ca}}{2\epsilon}\Delta P, \tag{2.29}$$

meaning centreline curvature depends on the pressure drop $\Delta P = P_+ - P_-$. Neighbouring foam bubbles are roughly equal, so $\Delta P << 1$ and may be set to 0. Then the centreline is linear in x:

$$H_0(x,t)=a(t)x+b(t), \tag{2.30}$$

so by a time-dependent rotation, we may set $H_0(x,t)\equiv 0$.

If instead we add (2.27) and (2.28), then recall (2.25), we obtain:

$$p_0(x,t)=2\frac{\partial w_0}{\partial z}-\frac{\epsilon}{2\mathrm{Ca}}\frac{\partial^2 h_0}{\partial x^2}=-2\frac{\partial u_0}{\partial x}-\frac{\epsilon}{2\mathrm{Ca}}\frac{\partial^2 h_0}{\partial x^2}, \tag{2.31}$$

where we have set $P_\pm = 0$ to determine p_0 up to a constant. At this point, no further progress can be made with $O(1)$ information only. Moreover, (NS1$O(\epsilon^2)$) and (NS2$zO(\epsilon^2)$) each contain two dependent variables with 1 subscripts that we have not yet considered. However, we may remove u_1 from (NS2$xO(\epsilon^2)$) by z-independence of p_0 and u_0, to get:

$$\left[\frac{\partial u_1}{\partial z}\right]_{z=-\frac{1}{2}h_0}^{z=\frac{1}{2}h_0}=\left[\left(\frac{\partial p_0}{\partial x}-\frac{\partial^2 u_0}{\partial x^2}\right)z\right]_{z=-\frac{1}{2}h_0}^{z=\frac{1}{2}h_0}=-3h_0\frac{\partial^2 u_0}{\partial x^2}-\frac{\epsilon}{2\mathrm{Ca}}h_0\frac{\partial^3 h_0}{\partial x^3}. \tag{2.32}$$

We may also evaluate u_{1_z} via (BC2$O(\epsilon^2)$) and (2.25), to obtain:

$$\left[\frac{\partial u_1}{\partial z}\right]_{z=-\frac{1}{2}h_0}^{z=\frac{1}{2}h_0}=\left[-\frac{\partial w_0}{\partial x}\right]_{z=-\frac{1}{2}h_0}^{z=\frac{1}{2}h_0}+4\frac{\partial h_0}{\partial x}\frac{\partial u_0}{\partial x}=h_0\frac{\partial^2 u_0}{\partial x^2}+4\frac{\partial h_0}{\partial x}\frac{\partial u_0}{\partial x}. \tag{2.33}$$

Merging (2.32), (2.33), we finally obtain:

Thin-film equations (TFEs)

$$\frac{\partial h_0}{\partial t}+\frac{\partial}{\partial x}\left(u_0 h_0\right)=0, \tag{TFE1}$$

$$\frac{\partial}{\partial x}\left(4h_0\frac{\partial u_0}{\partial x}\right)+\frac{\epsilon}{2\mathrm{Ca}}h_0\frac{\partial^3 h_0}{\partial x^3}=0. \tag{TFE2}$$

We note that this is a general configuration and the velocity scaling U_0 is still undetermined. It will transpire in later chapters as we balance desired physical effects.

2.7 Note on 3D thin-film equations

Schick [19] considers a more general derivation accounting for gravity and Marangoni stresses (σ-gradients) in 3D. With our configuration and a 3D-film $z(x,y,t) = H(x,y,t) \pm \frac{1}{2}h(x,y,t)$, conservation of mass (TFE1) becomes:

$$\frac{\partial h_0}{\partial t} + \frac{\partial}{\partial x}\left(u_0 h_0\right) + \frac{\partial}{\partial y}\left(v_0 h_0\right) = 0. \tag{2.34}$$

Meanwhile, manipulating the 3D-analogue of (BC1$O(1)$) gives Laplace's equation in the (x,y) plane:

$$\nabla^2 H_0 = \frac{\partial^2 H_0}{\partial x^2} + \frac{\partial^2 H_0}{\partial y^2} = 0. \tag{2.35}$$

Then, H_0 not necessarily flat as in the 2D-case, therefore an extra assumption to flatten the centreline is needed. Furthermore, (TFE2) has two counterparts due to the extra spatial dimension:

$$\frac{\partial}{\partial x}\left(4h_0\frac{\partial u_0}{\partial x} + 2h_0\frac{\partial v_0}{\partial y}\right) + \frac{\partial}{\partial y}\left(h_0\frac{\partial v_0}{\partial x} + h_0\frac{\partial u_0}{\partial y}\right) + \frac{\epsilon}{2\mathrm{Ca}}h_0\frac{\partial}{\partial x}\left(\frac{\partial^2 h_0}{\partial x^2} + \frac{\partial^2 h_0}{\partial y^2}\right) = 0, \tag{2.36}$$

$$\frac{\partial}{\partial x}\left(h_0\frac{\partial u_0}{\partial y} + h_0\frac{\partial v_0}{\partial x}\right) + \frac{\partial}{\partial y}\left(4h_0\frac{\partial v_0}{\partial y} + 2h_0\frac{\partial u_0}{\partial x}\right) + \frac{\epsilon}{2\mathrm{Ca}}h_0\frac{\partial}{\partial y}\left(\frac{\partial^2 h_0}{\partial x^2} + \frac{\partial^2 h_0}{\partial y^2}\right) = 0. \tag{2.37}$$

The system is evidently much more complex. For these reasons, and recalling the flow is mostly planar as in Figure 1.4, we maintain (TFE1)-(TFE2) and our 2D configuration.

Equipped with PDEs that describe free-films bounded by gas, we are ready to begin modelling lamella drainage.

Chapter 3

Breward & Howell's Model

3.1 Assumptions and configuration

In their work, Breward & Howell [7] make the following key assumptions:

(A1) (L) surfaces are almost flat and this region is dominated by viscous, as opposed to negligible capillary effects.
(A2) (PB) liquid velocity is negligible, so the region is treated as capillary-static; consequently, free surfaces here are shaped as circular arcs.

The reasoning behind **(A1)**-**(A2)** comes from experimental observations on parameter sizes for typical bubbles. Verification for typical parameters can be found in Appendix A.

The important consequence of **(A1)**-**(A2)** is that in (L)-(PB) flow, as viscous effects decrease and capillary increase, we expect a **transition region** (T) where both effects balance. Unlike (L) and (PB), this small (T) will not have any significance in the macroscopic foam geometry. Rather, it will serve a theoretical purpose, much akin boundary layers in singular perturbation theory, in order to match the solutions from (L) and (PB).

3.1.1 Lamella

We will model (L) in a 2D geometry using (TFE1)-(TFE2) from Chapter 2. Recalling **(A1)**, the second term of (TFE1) corresponding to capillary effects is negligible, i.e. $\epsilon/\mathrm{Ca} \ll 1$. Dropping 0 subscripts, we are left with:

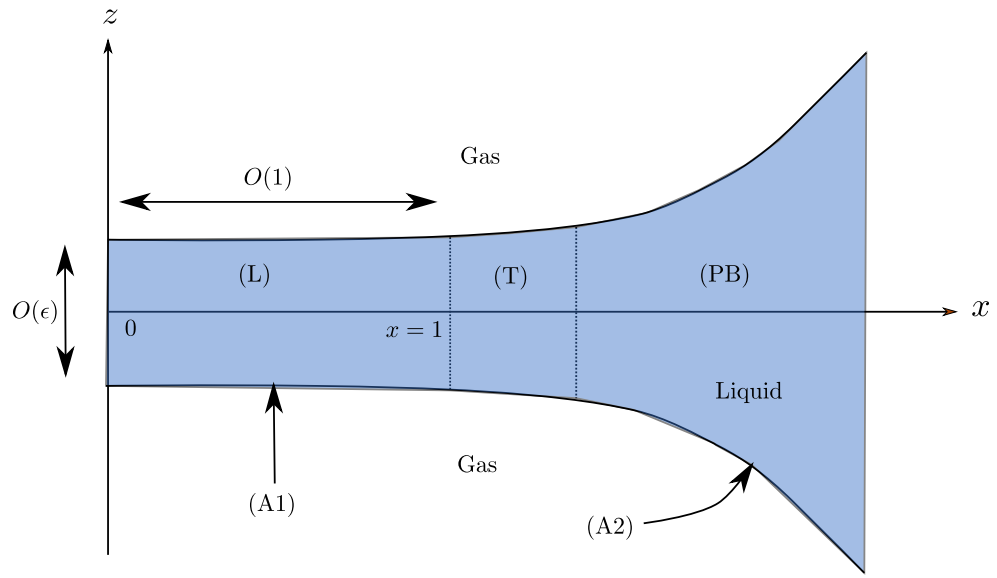

Figure 3.1: Non-dimensional problem and domain decomposition.

Lamella model

$$\frac{\partial h}{\partial t} + \frac{\partial}{\partial x}(uh) = 0, \tag{L1}$$

$$\frac{\partial}{\partial x}\left(4h\frac{\partial u}{\partial x}\right) = 0. \tag{L2}$$

In deriving these equations, we choose L_0 and h_0 (see (2.9)) to be the lamellar half-length (from its centre $x^\star = 0$ to the beginning of the transition region) and its initial thickness, respectively. The non-dimensional model configuration is pictured in Figure 3.1. We delay discussion of boundary condition to Section 3.2, until after we first consider the transition region.

3.1.2 Plateau border

In (PB), the assumption of small aspect ratio ϵ fails, since the film thickness becomes appreciables. Therefore, (TFE1)-(TFE2) are inapplicable. To illuminate **(A2)**, recalling pressure in gas bubbles is zero, we replace the lubrication scalings with:

(PB) nondimensionalisation

$$\begin{aligned} x^\star &= L_0 x, \quad & z^\star &= L_0 z, \\ u^\star &= U_0 u, \quad & w^\star &= U_0 w, \\ p^\star &= P_{PB}\, p, \quad & t^\star &= \tfrac{L_0}{U_0} t, \end{aligned} \tag{3.1}$$

where we have rescaled with a new P_{PB}, because pressure in the capillary-static (PB) has different behaviour to that in (L).

The normal stress (BC1*) on $z = \frac{h(x,t)}{2}$ is:

$$-P_{PB}\, p + \frac{\mu^\star U_0}{L_0}\left(\frac{u_x \frac{h_x^2}{4} \mp w_x \frac{h_x}{2} \mp u_z \frac{h_x}{2} + 2w_z}{1 + \frac{h_x^2}{4}}\right) = \frac{\sigma^\star}{L_0} \frac{\frac{h_{xx}}{2}}{(1 + \frac{h_x^2}{2})^{\frac{3}{2}}} \tag{3.2}$$

Recalling the definition $\mathrm{Ca} = \mu^\star U_0/\sigma^\star$, we rewrite (3.2):

$$-\left[\frac{P_{PB} L_0}{\sigma^\star}\right] p + \mathrm{Ca}\left(\frac{u_x \frac{h_x^2}{4} \mp w_x \frac{h_x}{2} \mp u_z \frac{h_x}{2} + 2w_z}{1 + \frac{h_x^2}{4}}\right) = \frac{\frac{h_{xx}}{2}}{(1 + \frac{h_x^2}{2})^{\frac{3}{2}}} \tag{3.3}$$

Crucially, $\mathrm{Ca} << 1$ (see Appendix A). In order to balance the first and third term in (3.3), we pick:

$$P_{PB} = \frac{\sigma^\star}{L_0}. \tag{3.4}$$

To leading order in Ca, evaluating κ at $z = \frac{h(x,t)}{2}$:

$$\kappa = -p(x,t), \tag{3.5}$$

meaning curvature is directly related to the pressure jump. For simplicity, we assume $p(x,t)$ is constant, although we will challenge this in Chapter 4. In our 2D geometry, this implies that PBs are constructed of circular arcs (via standard differential geometry calculations). We denote the radius by a_0, so the dimensional curvature is $\kappa = \frac{1}{a_0}$.

The newfound pressure scaling illuminates the direction of flow, since:

$$\frac{|P_{PB}|}{|P_0|} = \frac{\sigma^\star}{\mu^\star U_0} = \frac{1}{\mathrm{Ca}} \gg 1. \tag{3.6}$$

As pressure in (L) is 0 (due to $P = 0$ in gas bubbles and no curvature) and decreases as we move towards (T), the typical (PB) pressure is much more negative and drives flux of liquid out of (L).

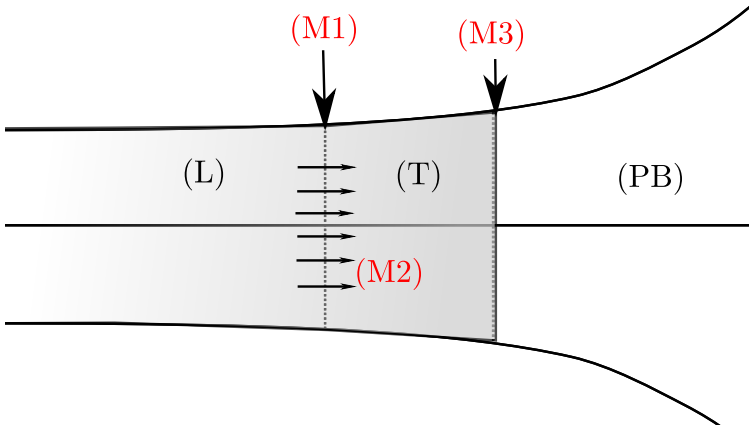

Figure 3.2: Geometric visualisation of **(M1)-(M3)**.

3.1.3 Transition region

Having conjectured the existence of (T), we now find its lengthscale. In our configuration, (T) is to the right of (L), so we shift coordinates using a **stretching parameter** δ. The dimensionless length in (T) becomes

$$x = \frac{L^\star(t^\star)}{L_0} + \delta\xi, \tag{3.7}$$

where $L^\star(t^\star)$ is the dimensional lamella half-length. We desire δ to be sufficiently small so that (T) does not interfere with macroscopic physics, but large enough for (TFE1)-(TFE2) to apply. We begin with the following qualitative observations:

Matching conditions

(M1) As we approach (L), the thickness of (T) must approach that of (L).
(M2) The flux of liquid leaving (L) must equal the flux entering (T).
(M3) As we approach (PB), the curvature of (T) must approach $\frac{1}{a_0}$.

We use **(M3)** to find δ. The dimensional curvature in (T) at the top surface becomes:

$$\frac{\frac{h^\star_{x^\star x^\star}}{2}}{\left(1+\frac{h^{\star 2}_{x^\star x^\star}}{4}\right)^{\frac{3}{2}}} = \frac{\frac{\epsilon}{2\delta^2 L_0}h_{\xi\xi}}{(1+\frac{\epsilon^2}{4\delta^2}h_\xi^2)^{\frac{3}{2}}} \sim \frac{\epsilon}{2\delta^2 L_0}h_{\xi\xi}, \tag{3.8}$$

provided $\epsilon/\delta \ll 1$ in the denominator. As $\xi \to +\infty$ and we move towards (PB), this needs to approach $\frac{1}{a_0}$. Therefore:

$$\delta = \frac{\sqrt{\epsilon a_0}}{\sqrt{2L_0}} = \frac{\sqrt{h_0 a_0}}{\sqrt{2}L_0} \ll 1. \tag{3.9}$$

The relationship (3.9) differs from the definition of δ in [7] by a factor of $\sqrt{2}$; there is a mistake in the authors' original calculations. Regardless, the key is that in (T) we have $h^\star \sim h_0$, $x^\star \sim \delta L_0 \xi$ (up to translation), so that the aspect ratio of (T) is $\epsilon/\delta = h_0/\delta L_0 = \sqrt{2\epsilon L_0/a_0} \ll 1$. We verify this with typical parameters for water in Appendix A. The implication is that (TFE1)-(TFE2) are still applicable for (T). Rescaling distance through (3.7), dropping 0's and abusing notation in writing $u(\xi,t) = u(x,t), h(\xi,t) = h(x,t)$, they become:

$$\frac{\partial h}{\partial t} + \frac{1}{\delta}\frac{\partial}{\partial \xi}(uh) = 0, \tag{3.10}$$

$$\frac{1}{\delta^2}\frac{\partial}{\partial \xi}\left(4h\frac{\partial u}{\partial \xi}\right) + \frac{\epsilon}{2\delta^3 \mathrm{Ca}} h\frac{\partial^3 h}{\partial \xi^3} = 0. \tag{3.11}$$

As (T) balances viscous and capillary effects, coefficients in (3.11) must be of same order. To this end, we set:

$$\mathrm{Ca} = \frac{\epsilon}{\delta} << 1, \tag{3.12}$$

since we previously remarked $\epsilon << \delta << 1$, which also implies $\epsilon << \mathrm{Ca} << 1$. This fits in perfectly with our previous observations: Ca is small enough for viscosity in Plateau borders to be negligible, whereas it is large enough for capillary effects to vanish in lamellae.

The only unknown scaling is our typical velocity U_0. This follows directly from the definition of Ca, since:

$$\frac{\epsilon}{\delta} = \mathrm{Ca} = \frac{\mu^\star U_0}{\sigma^\star}. \tag{3.13}$$

Hence, substituting (3.9) into (3.13), we find:

$$U_0 = \frac{\sigma^\star}{\mu^\star}\sqrt{\frac{2h_0}{a_0}}. \tag{3.14}$$

In summary, to leading order in δ, equations (3.10)-(3.11) read:

Transition region model

$$\frac{\partial}{\partial \xi}(uh) = 0, \tag{T1}$$

$$\frac{\partial}{\partial \xi}\left(4h\frac{\partial u}{\partial \xi}\right) + \frac{1}{2}h\frac{\partial^3 h}{\partial \xi^3} = 0. \tag{T2}$$

3.2 Analysis of the lamella model

Before we solve the (L)-(T)-(PB) model in Section 3.3, we analyse (L1)-(L2). We first classify the model, before deriving a remarkable result on the evolution of the lamella's thickness.

3.2.1 Classification of the system

We may integrate (L2) and rewrite (L1)-(L2) as:

$$\frac{\partial h}{\partial t} + \frac{\partial}{\partial x}(uh) = 0, \tag{3.15}$$

$$4h\frac{\partial u}{\partial x} = T(t). \tag{3.16}$$

Introducing vector variables $\mathbf{v}(x,t) = (u(x,t), h(x,t))^T$, $\mathbf{c}(t) = (0, \frac{1}{4}T(t))^T$ enables us to write this as a first-order quasilinear system:

$$\mathbf{A}(x,t)\frac{\partial \mathbf{v}}{\partial x} + \mathbf{B}(x,t)\frac{\partial \mathbf{v}}{\partial t} = \mathbf{c}, \tag{3.17}$$

where $\mathbf{A}(x,t)$ and $\mathbf{B}(x,t)$ are:

$$\mathbf{A} = \begin{pmatrix} h(x,t) & u(x,t) \\ h(x,t) & 0 \end{pmatrix} \text{ and } \mathbf{B} = \begin{pmatrix} 0 & 1 \\ 0 & 0 \end{pmatrix}. \tag{3.18}$$

Inverse slopes of characteristics ($\frac{dt}{dx} = \lambda$) satisfy the eigenvalue problem (see [17]):

$$det(\mathbf{B} - \lambda\mathbf{A}) = 0 \tag{3.19}$$

from where $\lambda \in \{0, \frac{1}{u(x,t)}\}$. Provided velocity is finite, we obtain two distinct eigenvalues, so the system is **hyperbolic**. We may find the left eigenvectors of $\mathbf{B} - \lambda\mathbf{A}$: $\ell_0^T = (0,1)$ and $\ell_{1/u}^T = (1,-1)$. However, it is not possible to integrate towards obtaining Riemann invariants in this situation.

Regardless, hyperbolic systems are better behaved than elliptic systems, because the Cauchy problem (3.17) with suitable Cauchy data is well-posed. Then, the Cauchy-Kovalevskaya theorem (see [17]) guarantees local uniqueness, provided coefficients are suitably analytic and the initial data is nowhere tangent to the characteristics ($t = \text{const}$ and $\dot{x} = u(x,t)$). We now consider conditions that accompany (3.17).

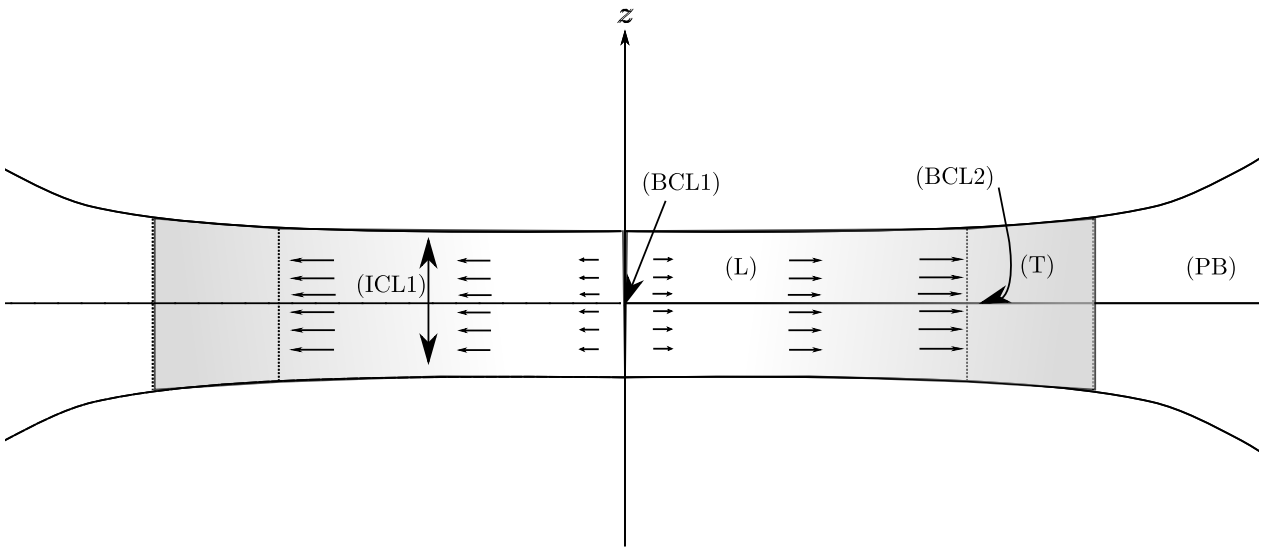

Figure 3.3: Geometric justification of ICs/BCs.

3.2.2 Spatially uniform evolution of lamella

The initial and boundary conditions for (L1)-(L2) read:

ICs/BCs for (L)

$$u(1,t)h(1,t) = Q(t), \qquad \text{(BCL1)}$$

$$u(0,t) = 0, \qquad \text{(BCL2)}$$

$$h(x,0) = h_0(x). \qquad \text{(ICL1)}$$

Justifying these is natural: (BCL1) is the statement of (M2), since flux leaving (L) equals that entering (T). Meanwhile, (BCL2) is a statement of symmetry: since we consider the lamella from its midpoint to the right, we can suppose there is a mirror image to the left, as shown in Figure 3.3. Consequently, liquid to the left of $x = 0$ moves leftwards and liquid to the right of $x = 0$ moves rightwards, implying $u(0,t) = 0$. Finally, (ICL1) represents the prescribed initial thickness of the lamella.

To further analyse (3.15)-(3.16), we note that (3.15) is reminiscent of the convective derivative of $h(x,t)$, off by a term hu_x. This suggests a change from Eulerian (x,t) to Lagrangian frame (X,τ), whereby instead of labelling points fixed in space, we fix coordinates with fluid particles at $t = 0$. The subsequent argument draws inspiration from Howell's analysis of fibres [13], but the configuration and the conclusion differ.

We define new coordinates X, τ:

Lagrangian specification

$$\begin{aligned} X &= x(X,0), \\ \frac{\partial x}{\partial \tau} &= u(x(X,\tau),t), \\ \tau &= t. \end{aligned} \tag{3.20}$$

Using the chain rule (and abuse of notation $h(x,t) = h(X,\tau)$) we find:

$$\frac{\partial h}{\partial \tau} = \frac{\partial h}{\partial t} + u\frac{\partial h}{\partial x}, \tag{3.21}$$

$$\frac{\partial u}{\partial x} = \frac{\partial}{\partial x}\left(\frac{\partial x}{\partial \tau}\right) = \frac{\partial^2 x}{\partial X \partial \tau}\frac{\partial X}{\partial x} = \frac{\partial^2 x}{\partial X \partial \tau}\left(\frac{\partial x}{\partial X}\right)^{-1}, \tag{3.22}$$

where the last equality follows from $x_X X_x = x_X X_x + x_\tau \tau_x = x_x = 1$. This enables us to rewrite (3.15)-(3.16) within the Lagrangian frame as:

$$\frac{\partial h}{\partial \tau} + h\frac{\partial^2 x}{\partial X \partial \tau}\left(\frac{\partial x}{\partial X}\right)^{-1} = 0, \tag{3.23}$$

$$h\frac{\partial^2 x}{\partial X \partial \tau}\left(\frac{\partial x}{\partial X}\right)^{-1} = T(\tau). \tag{3.24}$$

Multiplying through by $\frac{\partial x}{\partial X}$, equation (3.23) simplifies due to the product rule

$$\frac{\partial}{\partial \tau}\Bigg(\underbrace{h\frac{\partial x}{\partial X}}_{:= P(X)}\Bigg) = 0, \tag{3.25}$$

and we may therefore eliminate h entirely by plugging this into (3.24), obtaining

$$T(\tau) = P(X)\frac{\partial^2 x}{\partial X \partial \tau}\left(\frac{\partial x}{\partial X}\right)^{-2} = -\frac{\partial}{\partial \tau}\left[P(X)\left(\frac{\partial x}{\partial X}\right)^{-1}\right], \tag{3.26}$$

where the second manipulation only involves the chain rule.

If $\tilde{T}(\tau)$ is the antiderivative of $T(\tau)$ such that $\tilde{T}(0) = 0$, we may write:

$$\underbrace{P(X)\left(\frac{\partial x}{\partial X}\right)^{-1}}_{h(x,t)} = -\tilde{T}(\tau) + R(X), \tag{3.27}$$

where $R(X)$ appears after the integration.

To complete the argument, we set $\tau = t = 0$ and apply (ICL1), obtaining $R(X) = h_0(x)$. Consequently, by (3.27), (L) thinning is a linear superposition of two effects: one varying with space and the other with time. Recalling assumption **(A1)** and letting (L) be perfectly flat at $O(1)$ in ϵ gives $h_0(x) \equiv 1$. Under this configuration, the right-hand side of (3.27) is time-dependent only, resulting in:

Spatially uniform evolution

$$h(x,t) = h_L(t). \tag{3.28}$$

An alternative approach via a partial hodograph transformation, as employed by Dewynne et al. [10], yields the same result. The idea is to define a scaled impulse $J = \int_0^t T(t)dt$ and formally change to h and J as independent variables. We chose to present Howell's approach due to the physical interpretation of the coordinate change (3.20).

3.3 Solving the model

In total, our model comprises of two systems of coupled PDEs (L1)-(L2) and (T1)-(T2); three matching conditions (M1)-(M3); and three initial/boundary conditions (BCL1), (BCL2), (ICL1). Deciding where to start solving the model is therefore difficult. We present a schematic depicting the interplay between regions in Figure 3.4, emphasising that effects due to (PB) only appear through matching conditions for (T). We therefore consider (T) first and analyse (L) afterwards.

3.3.1 Transition region

We recall that the model in the transition region is

$$\frac{\partial}{\partial \xi}(uh) = 0, \tag{T1}$$

$$\frac{\partial}{\partial \xi}\left(4h\frac{\partial u}{\partial \xi}\right) + \frac{1}{2}h\frac{\partial^3 h}{\partial \xi^3} = 0, \tag{T2}$$

combined with:

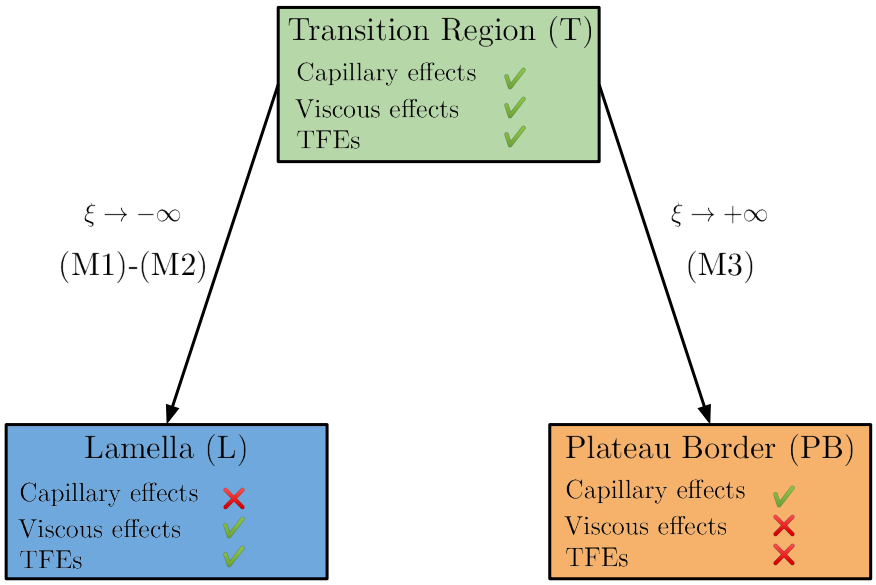

Figure 3.4: (T)'s relationship to (L) and (PB).

Matching conditions

$$h \to h_L(t) \text{ as } \xi \to -\infty, \tag{M1}$$

$$uh \to Q(t) \text{ as } \xi \to -\infty, \tag{M2}$$

$$h_{\xi\xi} \to 1 \text{ as } \xi \to +\infty. \tag{M3}$$

We begin by integrating (T1) and applying (M2), to find that:

$$u(\xi,t)h(\xi,t) = Q(t), \tag{3.29}$$

where the flux $Q(t)$ of liquid leaving (L) is unknown at present. We integrate (T2) by first noting the identity

$$h\frac{\partial^3 h}{\partial \xi^3} = \frac{\partial}{\partial \xi}\left(h\frac{\partial^2 h}{\partial \xi^2} - \frac{1}{2}\left(\frac{\partial h}{\partial \xi}\right)^2\right), \tag{3.30}$$

from where it follows that

$$4h\frac{\partial u}{\partial \xi} + \frac{1}{2}h\frac{\partial^2 h}{\partial \xi^2} - \frac{1}{4}\left(\frac{\partial h}{\partial \xi}\right)^2 = A(t), \tag{3.31}$$

where $A(t)$ appears from the integration. To simplify matters, we would like to remove u from (3.31). We differentiate (3.29), which yields:

$$\frac{\partial u}{\partial \xi} = -\frac{Q}{h^2}\frac{\partial h}{\partial \xi}. \tag{3.32}$$

Substituting this into (3.31) we find:

$$-\frac{4Q}{h^2}\frac{\partial h}{\partial \xi} + \frac{1}{2}h\frac{\partial^2 h}{\partial \xi^2} - \frac{1}{4}\left(\frac{\partial h}{\partial \xi}\right)^2 = A(t). \tag{3.33}$$

By (M1), $h_\xi \to 0$ and $h_{\xi\xi} \to 0$ as $\xi \to -\infty$ and hence $A(t) \equiv 0$. To integrate (3.31) once again, we note that the second and third term are reminiscent of the quotient rule and, upon multiplication by $h^{-\frac{3}{2}}$, (3.33) becomes:

$$\frac{\partial}{\partial \xi}\left(\frac{16}{3}\frac{Q}{h\sqrt{h}} + \frac{1}{\sqrt{h}}\frac{\partial h}{\partial \xi}\right) = 0. \tag{3.34}$$

Integrating (3.34) and determining the integration constant by applying (M1) gives:

$$\frac{1}{\sqrt{h}}\frac{\partial h}{\partial \xi} = \frac{16Q}{3}\left(\frac{1}{h_L\sqrt{h_L}} - \frac{1}{h\sqrt{h}}\right). \tag{3.35}$$

We next turn to (M3). As $\xi \to \infty$:

$$h \sim \frac{1}{2}\xi^2 \ , \ \frac{\partial h}{\partial \xi} \sim \xi. \tag{3.36}$$

Considering $\xi \to \infty$ and substituting (3.36) into (3.35), after rearranging we obtain:

$$Q(t) = \frac{3\sqrt{2}}{16}h_L(t)^{\frac{3}{2}}. \tag{3.37}$$

This is a physically significant insight: as the lamella thins, the amount of liquid flowing away from it decreases (as there is less liquid available).

We may go one step further and use (3.37) to simplify (3.35) as much as possible, finding that:

$$h\frac{\partial h}{\partial \xi} = \sqrt{2}\left(h^{\frac{3}{2}} - h_L^{\frac{3}{2}}\right), \tag{3.38}$$

To eliminate h_L from (3.38), we rescale variables:

$$\hat{h} = \frac{h}{h_L} \text{ and } \hat{\xi} = \frac{\xi}{\sqrt{h_L}}, \tag{3.39}$$

which gives:

$$\hat{h}\frac{\partial \hat{h}}{\partial \hat{\xi}} = \sqrt{2}\left(\hat{h}^{\frac{3}{2}} - 1\right). \tag{3.40}$$

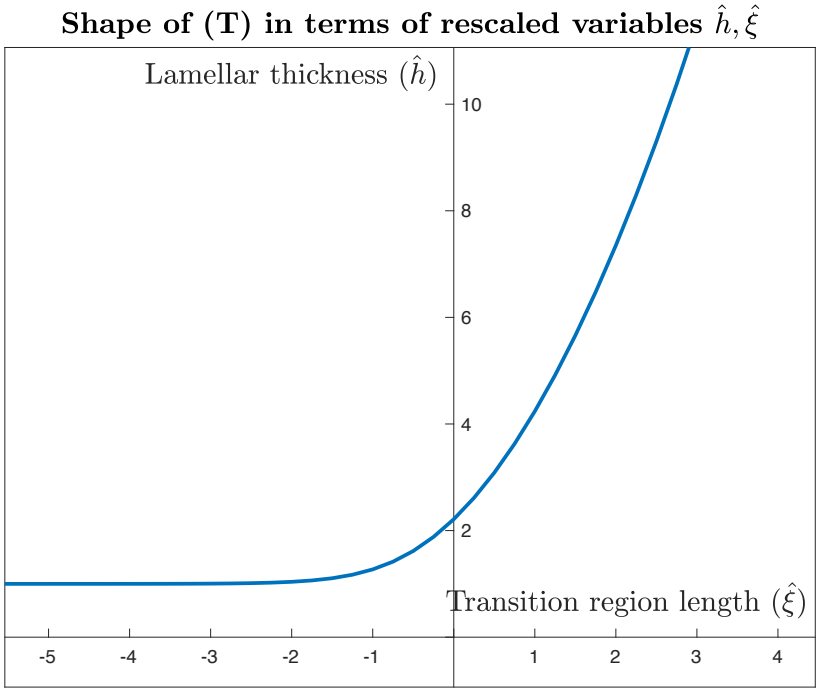

Figure 3.5: Tranisition region monotonic profile.

The absence of t derivatives enables this PDE to be solved by separation of variables. The result is an implicit solution for $\hat{h}$:

Explicit solution of the transition region

$$\sqrt{2}\hat{\xi} + \text{const} = 2\sqrt{\hat{h}} - \frac{2}{\sqrt{3}} \tan^{-1}\left(\frac{1+2\sqrt{\hat{h}}}{\sqrt{3}}\right) + \frac{1}{3}\log\left(\frac{1-2\sqrt{\hat{h}}+\hat{h}}{1+\sqrt{\hat{h}}+\hat{h}}\right). \tag{3.41}$$

where we may, without loss of generality, set the additive constant to be 0, since this corresponds to a shift in $\hat{\xi}$.

Figure 3.5 depicts this transition region profile. The result is what we expected all throughout: as $\xi \to -\infty$ (T) flattens to approach (L), whereas in approaching (PB) as $\xi \to \infty$, (T) must adjust to match its curvature.

3.3.2 Lamella

In Section 3.2 we showed that, under spatially uniform thickness initially, the lamella remains spatially uniform at all times. Writing $h(x,t) = h_L(t)$, our system (L1)-(L2)

becomes:

$$\frac{dh_L}{dt} + h_L \frac{\partial u}{\partial x} = 0, \tag{3.42}$$

$$h_L \frac{\partial^2 u}{\partial x^2} = 0, \tag{3.43}$$

with conditions:

$$u(1,t)h_L(t) = Q(t), \tag{BCL1}$$

$$u(0,t) = 0, \tag{BCL2}$$

$$h_L(0) = 1 \tag{ICL1}$$

Equation(3.43) tells us u is linear in x, and using (BCL1)-(BCL2) we obtain:

$$u(x,t) = \frac{Q(t)}{h_L(t)} x. \tag{3.44}$$

Substituting (3.44) into conservation of mass (3.42), we obtain a first-order IVP for $h_L(t)$, namely:

$$\frac{dh_L}{dt} = -Q(t), \tag{3.45}$$

subject to

$$h_L(0) = 1. \tag{3.46}$$

At first glance, (3.45) seems unsolvable due to $Q(t)$ dependence, yet (3.37) gives us a direct relationship between $Q(t)$ and $h_L(t)$. Therefore (3.45) becomes

$$\frac{dh_L}{dt} = -\frac{3\sqrt{2}}{16} h_L^{\frac{3}{2}}, \tag{3.47}$$

which can be solved immediately by separating variables to give:

$$\frac{1}{\sqrt{h_L}} = \frac{3\sqrt{2}}{32} t + 1, \tag{3.48}$$

where (3.46) determines the integration constant. Finally:

Evolution of (L) thickness (t^{-2} law)

$$h_L(t) = \frac{1}{\left(\frac{3\sqrt{2}}{32} t + 1\right)^2}. \tag{3.49}$$

An issue with (3.49) is that it takes infinitely long for the lamella to vanish, with no observable rupture as anticipated in Chapter 1. One explanation is that we have

neglected intermolecular forces, which we may circumvent by introducing a *critical thickness*: experimentally-supported $h_c^\star$ at which lamellae rupture. The dimensionless rupture time is given by rearranging (3.48):

$$t_c = \frac{32}{3\sqrt{2}}\left[\frac{1}{\sqrt{h_c}} - 1\right]. \tag{3.50}$$

Redimensionalising using (2.9) and (3.14), this becomes:

$$t_c^\star = \frac{16\mu^\star L_0\sqrt{a_0}}{3\sigma^\star}\left[\frac{1}{\sqrt{h_c^\star}} - \frac{1}{\sqrt{h_0}}\right]. \tag{3.51}$$

The prediction (3.51) is central, as it outputs a rupture time given initial parameters (see Appendix A for calculations).

Throughout our modelling, we have made numerous reasonable assumptions, perhaps the most courageous of which was **(A2)**, as justified below (3.5). In the next chapter, we investigate its validity and describe a distinguished limit whereby more caution is necessary.

Chapter 4

Brush & Davis' Model

Brush & Davis [8] build directly upon Breward & Howell's model, but argue that for very dry foams ($\phi < 0.02$), assumption **(A2)** breaks down and hence (M3) is no longer true. The results in this chapter are formally equivalent to those of these authors, but the notation and presentation is reconciled with Chapter 3. Moreover, the derivation in Section 4.2 is original, although (C1)-(C2) were presented in [8] in similar form.

4.1 Conservation laws

Reinforcing the assumption of negligible drainage perpendicular to the $(x^\star, z^\star)$-plane, we introduce (see Figure 4.1):

Brush & Davis' conservation laws

(C1) The liquid area stored in (L), (T) and (PB) is preserved.
(C2) The centrelines from the midpoint of (L) to the centres of neighbouring (PB) regions are of fixed length.

(C1) is intuitive, as the absence of a source/sink outside of our two-dimensional (L)-(T)-(PB) system implies conservation of matter in the plane. As the liquid's density $\rho^\star$ is constant, its area must be preserved. **(C2)** is related: in a symmetric configuration, all centrelines should be equal across different bubbles. Assume their length changes: as **(C1)** is obeyed, then the total liquid area, given by the sum of areas of the dashed polygons (built from centrelines) minus the constant area of incompressible gas, also changes. But this contradicts **(C1)**, so **(C2)** holds.

We will consider a periodic hexagonal structure, which is commonly observed as it satisfies **(P3)**, with three lamellae meeting at a border. Figure 4.2 illustrates how

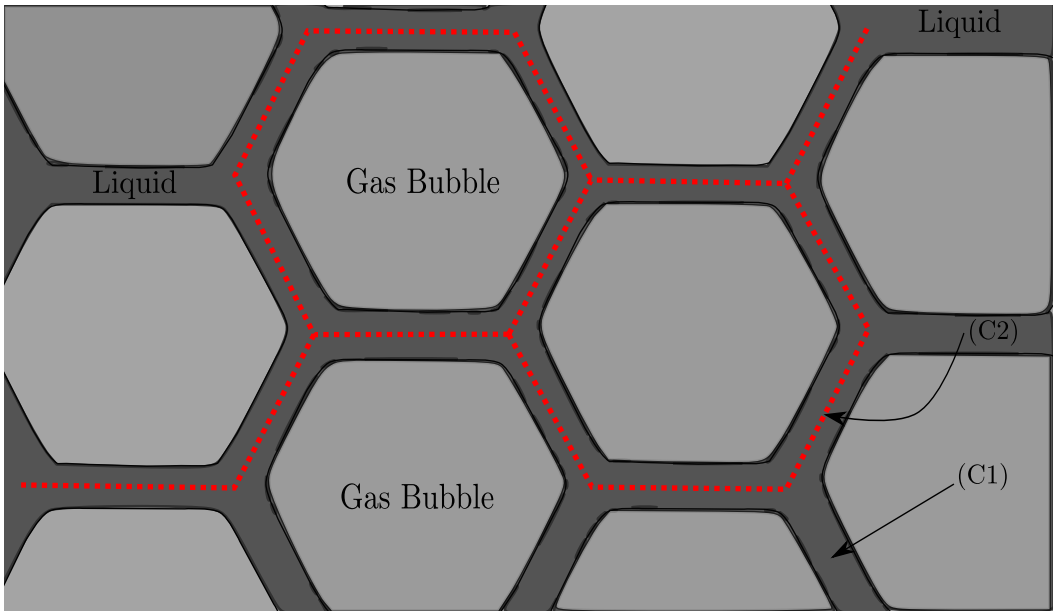

Figure 4.1: **(C1)** represents conservation of the black area, whereas **(C2)** is the preservation of the red dashed centrelines.

macroscopic foam is completely characterised by periodicity - subsequent arguments work for any regular polygon and we consider a general φ (for hexagons, $\varphi = \frac{\pi}{6}$). Using this decomposition, we may restrict ourselves to the thin-film as in Figure 4.3, to obtain a configuration akin that of Chapter 3. We let $A_L^\star$, $A_T^\star$, $A_{PB}^\star$ represent the dimensional (L), (T), and (PB) areas, respectively. We also define $d^\star$ to be the centreline length $|AD|$ in Figure 4.3.

We may therefore state precise formulations of **(C1)**-**(C2)**:

Conservation laws (periodic description)

(C1) $$\frac{d}{dt^\star}\left(A_L^\star + A_T^\star + A_{PB}^\star\right) = 0,$$

(C2) $$\frac{d}{dt^\star}\left(d^\star\right) = \frac{d}{dt^\star}\left(|AB| + |BC| + |CD|\right) = 0.$$

We next investigate how these laws change our understanding of the (L)-(PB)-(T) system, by deducing non-dimensional ODEs which give rise to distinguished regimes. We maintain **(A1)** from Chapter 3 and treat (PB) as capillary static, yet do not assume that $p(x,t)$ in (3.5) is constant. Consequently, all modelling from Chapter 3 is applicable except for curvature arguments, meaning results up until (3.35) hold.

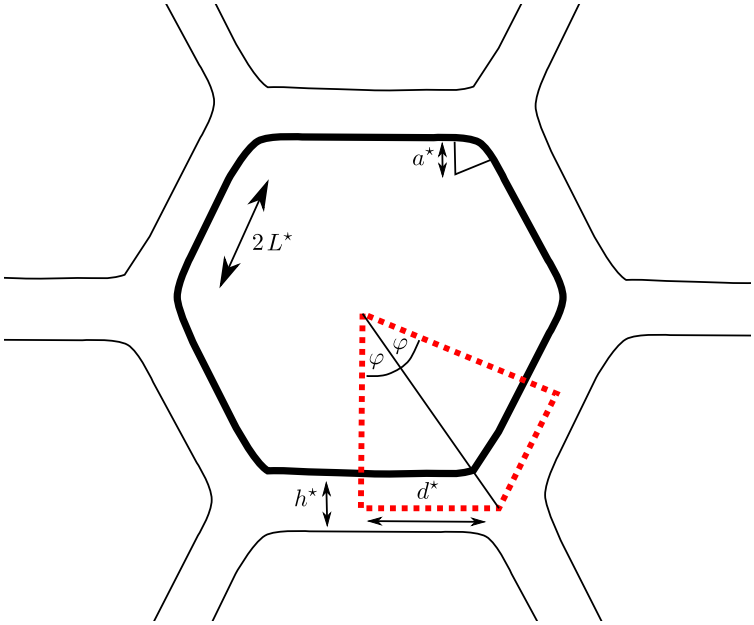

Figure 4.2: Periodic decomposition gives a macroscopic description of foam.

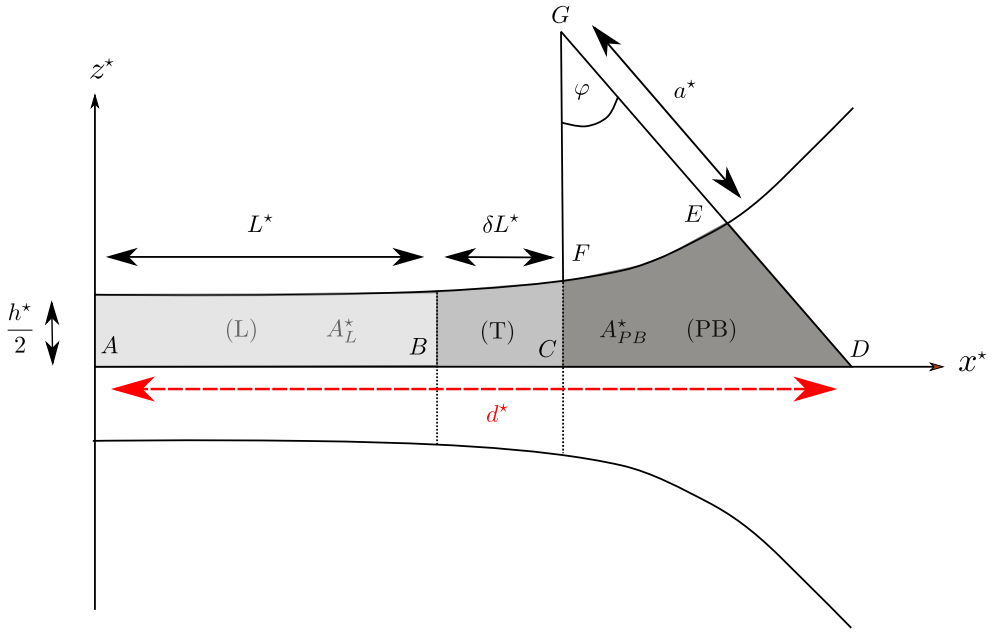

Figure 4.3: Geometric characterisation of the periodic decomposition.

4.2 Conservation equations

Refer to Figure 4.1. The contribution of (T) is $O(\delta)$ due to its lengthscale, so $A_T^\star$ is of higher order than $A_L^\star, A_{PB}^\star$ and may be neglected. Meanwhile, recalling spatial uniformity (3.28), we see:

$$A_L^\star = \frac{1}{2}\int_0^{L^\star(t^\star)} h_L^\star(t^\star)dx^\star = \frac{1}{2}L^\star(t^\star)h_L^\star(t^\star). \tag{4.1}$$

No integration would succeed in (PB) as we do not explicitly know $h^\star(x^\star, t^\star)$ there. Instead, $A_{PB}^\star$ can be found geometrically (see Figure 4.3):

$$A_{PB}^\star = |\triangle CDG| - |\triangledown GFE| = \frac{1}{2}\left(a^\star + \frac{1}{2}h_T^\star\right)(d^\star - L^\star - \delta L^\star) - \frac{a^{\star 2}\varphi}{2}, \tag{4.2}$$

where $h_T^\star$ is the thickness $|CF|$ of (T) at $\xi = \infty$. Next, elementary trigonometry in ΔCDG gives us:

$$d^\star = L^\star + \delta L^\star + \left(\frac{h_T^\star}{2} + a^\star\right)\tan\varphi. \tag{4.3}$$

This enables us to eliminate $d^\star$ from (4.2):

$$A_{PB}^\star = \frac{1}{2}\left(a^\star + \frac{h_T^\star}{2}\right)^2 \tan\varphi - \frac{a^{\star 2}\varphi}{2}. \tag{4.4}$$

In total, **(C1)** reads:

$$\frac{d}{dt^\star}\left(L^\star h_L^\star + \left(a^\star + \frac{h_L^\star}{2}\right)^2 \tan\varphi - a^{\star 2}\varphi\right) = 0. \tag{4.5}$$

To proceed further, we nondimensionalise:

Geometric nondimensionalisation

$$\begin{aligned} a^\star(t^\star) &= a_0 a(t), \quad a^\star(0) = a_0; \\ h^\star(t^\star) &= h_0 h(t), \quad h^\star(0) = h_0; \\ L^\star(t^\star) &= L_0 L(t), \quad L^\star(0) = L_0; \\ t^\star &= \tfrac{L_0}{U_0} t. \end{aligned} \tag{4.6}$$

Applying these scalings to (4.5):

$$L_0 h_0 \frac{d(Lh_L)}{dt} + a_0 h_0 \tan\varphi \frac{d(ah_T)}{dt} + \frac{h_0^2}{4}\frac{d(h_T^2)}{dt} + a_0^2(\tan\varphi - \varphi)\frac{d(a^2)}{dt} = 0. \tag{4.7}$$

We recall δ from (3.9):

$$\delta = \frac{\sqrt{h_0 a_0}}{\sqrt{2}L_0}, \tag{4.8}$$

to obtain $a_0 h_0 = 2\delta^2 L_0^2$, further noting that $h_0^2 = \epsilon^2 L_0^2$. Therefore, the second and third terms of (4.7) are negligible (as expected since $|CF| \ll |FG|$). This leaves us with:

$$\left[\frac{L_0 h_0}{a_0^2}\right]\frac{d(Lh_L)}{dt} = (\varphi - \tan\varphi)\frac{d(a^2)}{dt}. \tag{C1}$$

Moreover, **(C2)** gives:

$$\frac{d}{dt^\star}(d^\star) = \frac{d}{dt^\star}\left(L^\star + \delta L^\star + \left(\frac{h_T^\star}{2} + a^\star\right)\tan\varphi\right) = 0. \tag{4.9}$$

Dropping the term with δ coefficient, upon nondimensionalisation we obtain:

$$\frac{dL}{dt} = -\left[\frac{a_0}{L_0}\right]\frac{da}{dt}\tan\varphi - \left[\frac{h_0}{2L_0}\right]\frac{dh_T}{dt}\tan\varphi. \tag{4.10}$$

Multiplying the above by $a_0 L_0$ and again noting $a_0 h_0 = 2\delta^2 L_0^2$, the rightmost term may be neglected. We finally write:

Nondimensional **(C1)-(C2)**

$$\left[\frac{L_0 h_0}{a_0^2}\right]\frac{d(Lh_L)}{dt} = (\varphi - \tan\varphi)\frac{d(a^2)}{dt}, \tag{C1}$$

$$\frac{dL}{dt} = -\left[\frac{a_0}{L_0}\right]\frac{da}{dt}\tan\varphi. \tag{C2}$$

Brush & Davis' work has $\sin\varphi$ instead of $\tan\varphi$: this is a typographical error and is corrected in subsequent papers (see [9]).

4.3 Distinguished limits

Having obtained (C1)-(C2), we derive a thinning law analogous to (3.49). In (C1)-(C2), only the two bracketed fractions depend on parameter sizes. Distinct cases arise when either is $O(1)$.

4.3.1 Semi-dry foam

We first consider the case when

$$\frac{a_0}{L_0} \sim O(1). \tag{4.11}$$

From (4.1) and (4.4), we see $A_L^\star/L_0 \sim O(\epsilon)$, whereas $a_0/L_0 \sim O(1)$ tells us $A_{PB}^\star/L_0 \sim O(1)$. Meanwhile, the fraction of area of the polygonal gas bubble (proportional to

L_0) is $O(1)$. Therefore, much more liquid area is concentrated in (PB) as opposed to (L), and the liquid in (PB) strikes a balance with the gas area. We henceforth classify this as **semi-dry foam**.

Next, the other bracketed quantity becomes (recalling $h_0 = \epsilon L_0$):

$$\frac{L_0 h_0}{a_0^2} = \epsilon \left(\frac{L_0}{a_0}\right)^2 \sim O(\epsilon). \tag{4.12}$$

The (T) stretching parameter is:

$$\delta = \frac{\sqrt{h_0 a_0}}{\sqrt{2} L_0} = \frac{\sqrt{\epsilon}}{\sqrt{2}} \times \sqrt{\frac{a_0}{L_0}} \sim O(\sqrt{\epsilon}). \tag{4.13}$$

From (4.12), (C1) simplifies greatly at leading order, yielding:

$$a(t) = a(0) = 1. \tag{4.14}$$

Consequently, the right-hand side of (C2) vanishes, hence:

$$L(t) = L(0) = 1. \tag{4.15}$$

Crucially, (4.14) and (4.15) confirm all the assumptions of Chapter 3, so this limit is equivalent to Breward & Howell's work.

4.3.2 Dry foam

We next consider the case:

$$\frac{L_0 h_0}{a_0^2} \sim O(1). \tag{4.16}$$

As $h_0 = \epsilon L_0$, we have:

$$\left(\frac{a_0}{L_0}\right)^2 = \frac{a_0^2}{L_0 h_0} \times \epsilon \sim O(\epsilon), \tag{4.17}$$

thus $\frac{a_0}{L_0} \sim O(\sqrt{\epsilon})$. Therefore, we obtain $A_L^\star / L_0 \sim O(\epsilon)$ and $A_{PB}^\star / L_0 \sim O(\epsilon)$. Consequently, there is a balance between liquid area in (L) and (PB), which is negligible compared to the gas area. We classify this as **dry foam**.

Equation (4.17) helps us simplify (C2), which at $O(1)$ again gives $L(t) = 1$. However, the curvature change is non-trivial, and with the definition $\omega = \tan\varphi - \varphi$, (C1) becomes:

$$\frac{dh_L}{dt} = -\frac{\omega a_0^2}{L_0 h_0} \frac{d(a^2)}{dt}. \tag{4.18}$$

This is easily integrable: using $h_L(0) = 1$, $a(0) = 1$, we obtain:

(PB) radius evolution

$$a(t) = \sqrt{1 + \frac{L_0 h_0}{\omega a_0^2}\Big(1 - h_L(t)\Big)}. \tag{4.19}$$

For the remainder of the essay we will work with hexagons, so $\omega = \tan\frac{\pi}{6} - \frac{\pi}{6} \approx 0.054 > 0$. This means that as (L) thins, $a(t)$ will be steadily increasing. In other words, the pressure drop in (3.5) will vary, rendering our initial assumption $p(x,t) =$ constant invalid for this configuration.

We proceed to obtain the desired law of thinning. By matching (L) and (T) from Chapter 3, we still have:

$$\frac{dh_L}{dt} = -Q(t) \tag{4.20}$$

Again, we want to express $Q(t)$ in terms of $h_L(t)$ and solve (4.20). However, as $a(t)$ is no longer fixed, we need to revisit Chapter 3 and generalise calculations for varying $a(t)$. As we suggested earlier, only (M3) changes, as the dimensional curvature in (3.8) now approaches $\frac{1}{a^\star(t^\star)}$ as $\xi \to \infty$. Nondimensionalising, this gives:

$$\frac{\partial^2 h}{\partial \xi^2} \to \frac{a_0}{a^\star(t^\star)} = \frac{1}{a(t)} \text{ as } \xi \to \infty. \tag{M3'}$$

Proceeding, calculations through (3.29)-(3.35) to match the flux and the curvature are identical (as they only utilise $\xi \to -\infty$), yielding:

$$\frac{1}{\sqrt{h}}\frac{\partial h}{\partial \xi} = \frac{16Q(t)}{3}\left(\frac{1}{h_L\sqrt{h_L}} - \frac{1}{h\sqrt{h}}\right). \tag{4.21}$$

However, (M3') now tells us that, as $\xi \to \infty$:

$$h \sim \frac{1}{2a(t)}\xi^2 \ , \ \frac{\partial h}{\partial \xi} \sim \frac{1}{a(t)}\xi. \tag{4.22}$$

Hence, letting $\xi \to \infty$ in (4.21), we find:

$$Q(t) = \frac{3\sqrt{2}}{16}\left(\frac{h_L(t)^3}{a(t)}\right)^{\frac{1}{2}}. \tag{4.23}$$

It only remains to remove dependence on $a(t)$ in the flux via (4.19). For notational simplicity define:

$$\frac{1}{\tilde{w}} = \frac{L_0 h_0}{a_0^2 \omega}. \tag{4.24}$$

Then, we use the rescaling:

$$\tilde{h}_L = \frac{1}{1+\tilde{\omega}} h_L, \tag{4.25}$$

so that (4.19) simplifies to:

$$a(t) = (1+\tilde{\omega})^{\frac{1}{2}} \tilde{\omega}^{-\frac{1}{2}} \sqrt{1-\tilde{h}_L}. \tag{4.26}$$

Further, to eliminate $\tilde{\omega}$ from our ODE, we compress time:

$$\tilde{t} = \frac{3\sqrt{2}}{16}(1+\tilde{\omega})^{\frac{1}{4}} \tilde{\omega}^{\frac{1}{4}} t. \tag{4.27}$$

Combining (4.20) and (4.23), we are left with:

$$\frac{d\tilde{h}_L}{d\tilde{t}} = -\tilde{h}_L^{\frac{3}{2}} (1-\tilde{h}_L)^{-\frac{1}{4}}. \tag{4.28}$$

To express the solution, we introduce Gauss' hypergeometric function (convergent for $|z| < 1$):

$$F(a,b,c;z) = \sum_{n=0}^{\infty} \frac{(a)_n (b)_n}{(c)_n} \frac{z^n}{n!}, \tag{4.29}$$

where $(q)_n$ is the Pochhammer symbol (see [2]):

$$(q)_n = \begin{cases} 1 & n = 0 \\ q(q+1)...(q+n-1) & n > 0 \end{cases} \tag{4.30}$$

Using a computational engine (WolframAlpha/Mathematica), the implicit solution of (4.28) for $\tilde{h}_L$ finally becomes:

Dry foam thinning

$$\tilde{t} = \frac{2(1-\tilde{h}_L)^{\frac{1}{4}} + \tilde{h}_L F(\frac{1}{2}, \frac{3}{4}, \frac{3}{2}; \tilde{h}_L)}{\sqrt{\tilde{h}_L}} + \frac{2(1-\tilde{h}_L(0))^{\frac{1}{4}} + \tilde{h}_L(0) F(\frac{1}{2}, \frac{3}{4}, \frac{3}{2}; \tilde{h}_L(0))}{\sqrt{\tilde{h}_L(0)}}. \tag{4.31}$$

We plot the result in the $(\tilde{t}, \tilde{h})$-plane, and using (4.19), we may also visualise the evolution of the curvature radius on the same axes. Instead of using (4.31), we solve (4.28) using numerical methods, as MATLAB gives no explicit solution in terms of (4.29). All numerical solutions are produced using MATLAB's versatile **'ode45'** nonstiff solver and code is in Appendix B. In generating these, we set $L_0 h_0 / a_0^2 = 1$, so that $\tilde{\omega} = \omega$.

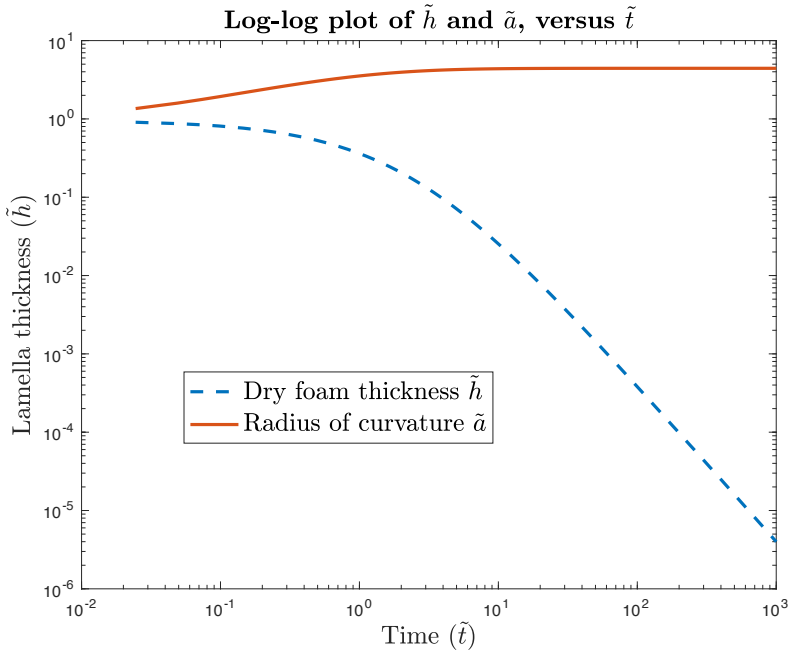

Figure 4.4: (PB) in dry foams becomes more curved as (L) thins.

4.4 Comparing the regimes

The following table summarises the limits considered.

Semi-dry versus dry foam				
Foam Type	$A_L^\star/L_0$	$A_{PB}^\star/L_0$	$a^\star(t^\star)/L_0$	$A_{liquid}^\star/A_{gas}^\star$
Semi-Dry ($\frac{a_0}{L_0} \sim O(1)$)	$O(\epsilon)$	$O(1)$	$O(1)$, constant	$O(1)$
Dry ($\frac{L_0 h_0}{a_0^2} \sim O(1)$)	$O(\epsilon)$	$O(\epsilon)$	$O(\sqrt{\epsilon})$, increasing	$O(\epsilon)$

To directly compare the regimes on same axes, we convert Breward & Howell's model to dry foam variables $(\tilde{t}, \tilde{h})$. Namely, (3.47) can be rewritten as:

$$\frac{d\tilde{h}_L}{d\tilde{t}} = -\frac{(1+\tilde{\omega})^{\frac{1}{4}}}{\tilde{\omega}^{\frac{1}{4}}}\tilde{h}_L^{\frac{3}{2}} \tag{4.32}$$

Finally, recalling the definition (4.27), (3.49) becomes

$$\tilde{h}_L(\tilde{t}) = \frac{\tilde{h}_L(0)}{\left(1 + \dfrac{\tilde{t}}{2\tilde{\omega}^{\frac{1}{4}}(1+\tilde{\omega})^{\frac{1}{4}}}\right)^2}. \tag{4.33}$$

From Figure 4.5, we may be misled into concluding that if L_0 and ϵ are the same, thinning is slower for dry foams. However, this is only true in dimensionless variables:

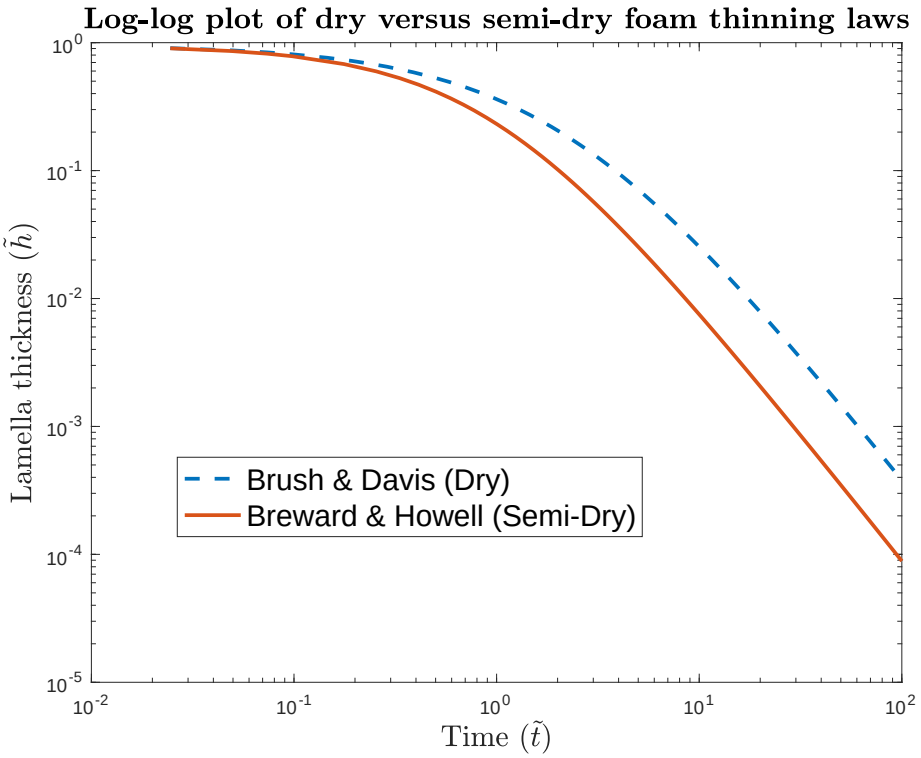

Figure 4.5: Nondimensional thinning for dry and semi-dry foams.

the smaller a_0 for dry foams greatly increases the velocity scaling (3.14), which upon redimensionalisation causes dry foams to rupture quicker. This paradox is illustrated with real parameters in Appendix A.2. Regardless, this plot demonstrates that the at large t, dry foam follows roughly the same t^{-2} law as semi-dry foam. Namely, as $t \to \infty$, $h_L \to 0$ and so $a(t) \to (1+\tilde{\omega})^{\frac{1}{2}}\tilde{\omega}^{-\frac{1}{2}}$, meaning the change in curvature eventually becomes negligible and both regimes decay approximately equally fast.

Chapter 5

Bubble Drainage & Surfactants

Having introduced the main models, we temporarily shift focus for two reasons. Firstly, in Section 5.1, we demonstrate that our modelling is directly applicable to a seemingly unrelated industrial problem, studied by Howell [14]. Secondly, in Section 5.2, we overview an early model of foam drainage accounting for surfactants [20], as a stepping stone towards more sophisticated approaches in the final chapter.

5.1 Draining of 2D bubbles

In molten glass manufacturing, melting of sand batch and contamination form small gas bubbles that rise to the glass surface. Understanding their stability is therefore crucial to quality assurance throughout production. This section sketches a particular model which gives a law of thinning for such bubbles, demonstrating extraordinary similarities with our models for foam.

5.1.1 Configuration

As the bubble rises, it forms a thin-film with the surface, giving a free-boundary problem in the $(x^\star, z^\star)$-plane with free surface $z^\star = F^\star(x^\star)$ such that $F^\star \to 0$ as $x \to \infty$ as in Figure 5.1. The pressures $P^\star_{atm}, P^\star_{bub}$ and $P^\star_{fluid}$ are all assumed constant. Moreover, the top film has constant surface tension $2\sigma^\star$ due to the inside and outside surfaces, whereas the remaining surfaces have surface tension $\sigma^\star$ (see Figure 5.2). Finally, the Navier-Stokes equations (NS1*)-(NS2*) are modified to include gravity.

The problem is then decomposed as in Figure 5.1:

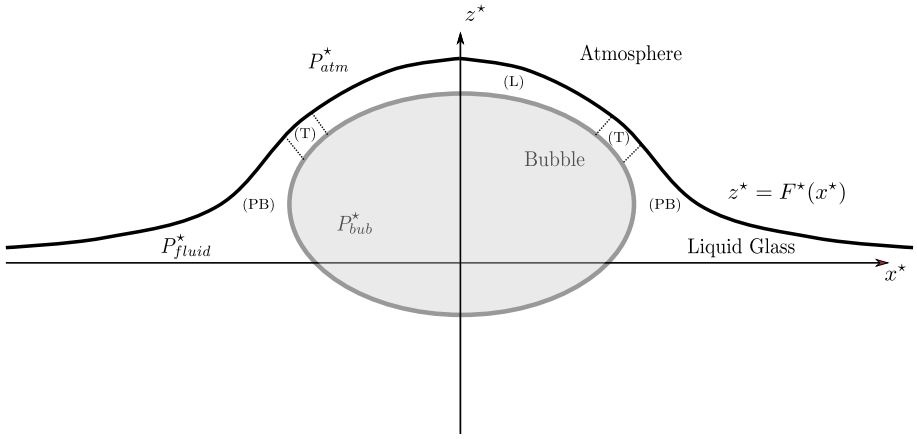

Figure 5.1: Molten glass problem. The domain decomposition uses nomenclature from foam.

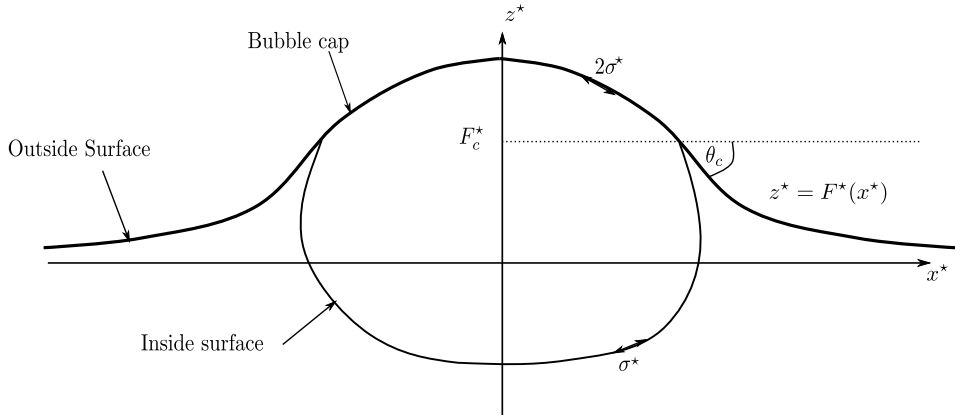

Figure 5.2: Capillary-static problem.

1. **Capillary-static region**: static regime where film has zero thickness and drainage outside its edge is governed by capillary-statics (*cf.* **Plateau border** in foam).

2. **Thin-film**: curved region of thickness $h^\star$ with aspect ratio $\epsilon << 1$, capping the bubble (*cf.* **lamellae** in foam).

3. **Transition region**: matching the solutions from the first two regions.

5.1.2 Capillary-static problem

By the Young-Laplace equation, we relate the constant curvature radius to hydrostatic pressure jumps:

$$a_0 = \frac{2\sigma^\star}{P^\star_{bub} - P^\star_{atm}}. \tag{5.1}$$

To measure gravitational effects, we define a Bond number:

$$B = \frac{\rho g^\star a_0^2}{\sigma^\star} = \frac{4\rho^\star g^\star \sigma^\star}{(P^\star_{bub} - P^\star_{atm})^2}. \tag{5.2}$$

Howell uses further applications of Young-Laplace to relate the angle at intersection θ_c to the corresponding height (see Figure 5.2):

$$F_c = -\frac{2}{\sqrt{B}} \sin\left(\frac{\theta_c}{2}\right), \tag{5.3}$$

as well as a_0 to the bubble's area $A^\star$:

$$\frac{A^\star}{a_0^2} = \sin\theta_c - \theta_c - 2\sin\theta_c \left[\sin\left(\frac{\theta_c}{2}\right) - \frac{1}{\sqrt{B}}\right]^2. \tag{5.4}$$

Subsequent asymptotic analysis gives (details in [14]):

$$\theta_c \sim -\frac{\pi}{8}B - \frac{3\pi}{32}B^2 + \frac{\pi^2}{32}B^{\frac{5}{2}} + O(B^3), \tag{5.5}$$

$$\frac{A^\star}{a_0^2} \sim \frac{\pi}{4} + \frac{\pi}{8}B - \frac{\pi^2}{32}B^{\frac{3}{2}} + O(B^2). \tag{5.6}$$

5.1.3 Thin-film problem

Using an arclength ($s^\star$) parametrisation the nondimensionalisation with unknown U_0 reads:

$$\begin{aligned} h^\star &= h_0 h, \quad s^\star = a_0 s, \\ u^\star &= U_0 u, \quad t^\star = \tfrac{a_0}{U_0} t. \end{aligned} \tag{5.7}$$

The governing equations become:

Bubble equations

$$\frac{\partial h}{\partial t} + \frac{\partial}{\partial s}(uh) = 0, \tag{BUB1}$$

$$\frac{\partial}{\partial s}\left(4h\frac{\partial u}{\partial s}\right) + \frac{\epsilon}{2\mathrm{Ca}} h\left(\frac{\partial^3 h}{\partial s^3} + \left(\frac{\partial \theta}{\partial s}\right)^2 \frac{\partial h}{\partial s}\right) = \frac{B}{\mathrm{Ca}} h \sin\theta, \tag{BUB2}$$

$$\left(1 + 2\epsilon \mathrm{Ca} h \frac{\partial u}{\partial s}\right)\frac{\partial \theta}{\partial s} = -1 + \frac{\epsilon B}{2} h\cos\theta, \tag{BUB3}$$

where $\epsilon = h_0/a_0 << 1$.

Equation (BUB1) is conservation of mass (*cf.* (TFE1) in foam) and (BUB2) represents shear stress, just like (TFE2). If gravity is negligible ($B = 0$), then it can be shown

$F^\star \equiv 0$ and $\theta_c = 0$ from (5.5). In this case, the bubble is circular from (5.6), (BUB3) no longer holds and $s^\star = x^\star$, so our equations reduce to (TFE1)-(TFE2). However, for $B \neq 0$, the film's curvature introduces a third PDE, namely (BUB3), representing normal stress. Regardless, the recipe for solving remains the same as that in Chapter 3, ultimately yielding:

Bubble t^{-2} law

$$\frac{h^\star(t^\star)}{h_0} = \frac{1}{\left(1 + \dfrac{32\sigma^{\star 2}}{3\pi\mu^\star\rho^\star g^\star}\sqrt{\dfrac{h_0}{a_0^7}}t^\star\right)^2}. \tag{5.8}$$

We therefore observe the same t^{-2} thinning as foam in previous chapters.

5.2 Surfactant Modelling

Having considered an application of our modelling outside of foam dynamics, we return to the challenge of understanding surfactants. Surfactant molecules tend to reside at interfaces, acting to reduce/increase surface tension. In turn, the resulting surface tension gradients cause shear stress, so (BC2*) from Chapter 2, which assumes zero tangential force, breaks down. We consider a simple model due to Schwartz & Princen [20].

5.2.1 Domain decomposition

We first decompose foams into four regions (Figure 5.3):

1. **Border region** of constant curvature radius a_0, moving away from the film with velocity $U^\star(t^\star)$.
2. **Transition region** matching (PB) with laid-down film.
3. **Laid-down film** with small interface slope, governed by lubrication equations.
4. **Black film**: Stagnant and very thin, governed by intermolecular forces.

5.2.2 Reduction to a governing PDE

We derive a lubrication-style PDE for the laid-down film, essentially compressing (TFE1)-(TFE2) into one equation for this configuration. In the notation of Chapter 2, (NS1), (NS2x), and (NS2z) remain the same, but boundary conditions change.

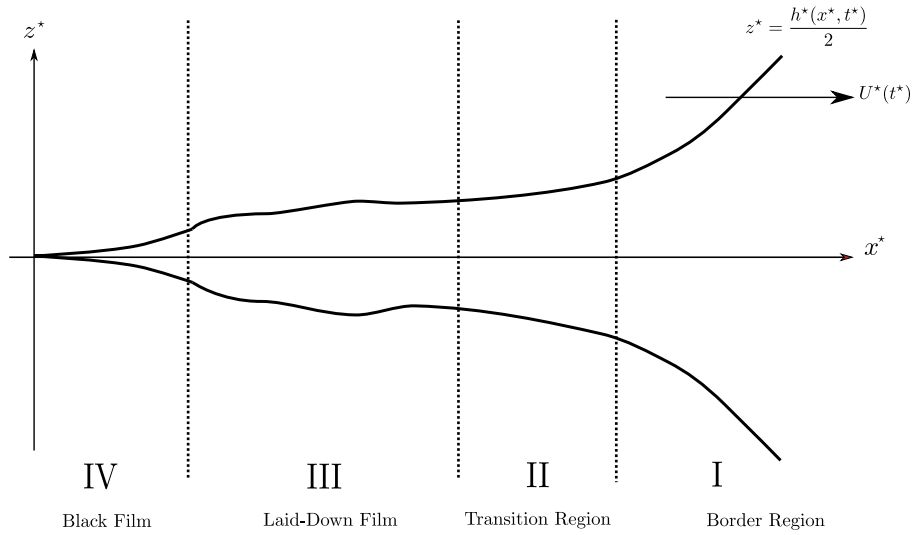

Figure 5.3: Schwartz & Princen's decomposition.

The authors assume that the surface is loaded with surfactant based on experimental observations of Mysels and Cox [15]. This bypasses σ-gradients and justifies a **no-slip** condition, effectively treating the interfaces as rigid walls. Therefore, instead of (BC2*), we impose:

$$u^\star = 0 \text{ on } z^\star = f^\star(x^\star, t^\star). \tag{5.9}$$

Schwartz & Princen further force $H(x,t) \equiv 0$ by symmetry (*cf.* Chapter 2, where we explicitly derived this). Note that the pressure scale (2.13) accompanied by (5.9) reduces (NS2$xO(1)$) to a triviality. To balance viscous and pressure terms, we set:

$$P_0 = \frac{\mu^\star U_0}{\epsilon^2 L_0}. \tag{5.10}$$

Nondimensionalising and assuming that Ca $\sim O(\epsilon^3)$ for capillary effects to appear, the governing equations become (*cf.* (NS1$O(1)$)-(NS2$zO(1)$)):

$$\frac{\partial u}{\partial x} + \frac{\partial w}{\partial z} = 0, \tag{5.11}$$

$$\frac{\partial^2 u}{\partial z^2} = \frac{\partial p}{\partial x}, \tag{5.12}$$

$$\frac{\partial p}{\partial z} = 0, \tag{5.13}$$

with boundary conditions on $z = \pm\dfrac{h(x,t)}{2}$:

$$p = -\frac{\epsilon^3}{2\mathrm{Ca}}\frac{\partial^2 h}{\partial x^2}, \tag{5.14}$$

$$u = 0, \tag{5.15}$$

$$w = \pm\frac{1}{2}\left(\frac{\partial h}{\partial t} + u\frac{\partial h}{\partial x}\right) = \pm\frac{1}{2}\frac{\partial h}{\partial t}. \tag{5.16}$$

The authors also impose a fourth condition due to symmetry about the x-axis:

$$\frac{\partial u}{\partial z} = 0 \text{ on } z = 0. \tag{5.17}$$

By (5.13), $p = p(x,t)$, so (5.14) describes pressure completely. Integrating (5.12) twice and applying (5.15) and (5.17), we obtain:

Parabolic velocity profile

$$u(x,z,t) = \frac{\epsilon^3}{4\mathrm{Ca}}\frac{\partial^3 h}{\partial x^3}\left(\frac{h^2}{4} - z^2\right). \tag{5.18}$$

We may contrast this with the velocity profile $u = u(x,t)$ in the surfactant-free configuration. Clearly, surfactant presence retards flow as manifested through the no-slip condition. Moreover, defining cross-layered average velocity:

$$\bar{u} = \frac{1}{h}\int_{-\frac{h}{2}}^{\frac{h}{2}} u(x,z,t)dz, \tag{5.19}$$

we may integrate (5.11) and use the Leibniz rule:

$$0 = \frac{\partial}{\partial x}\left(\int_{-\frac{h}{2}}^{\frac{h}{2}} u dz\right) - \frac{\partial h}{\partial x}\left[u\left(x,\frac{h}{2},t\right) + u\left(x,-\frac{h}{2},t\right)\right] + \left[w\right]_{-\frac{h}{2}}^{\frac{h}{2}}. \tag{5.20}$$

Recalling (5.15)-(5.16) gives conservation of mass:

$$\frac{\partial h}{\partial t} + \frac{\partial}{\partial x}\left(\bar{u}h\right) = 0. \tag{5.21}$$

Finally, we integrate (5.18) to obtain $\bar{u}$ and hence:

Lubrication PDE for laid-down region

$$\frac{\partial h}{\partial t} + \frac{\epsilon^3}{24\mathrm{Ca}}\frac{\partial}{\partial x}\left(h^3\frac{\partial^3 h}{\partial x^3}\right) = 0. \tag{5.22}$$

The model is solved by changing coordinates to the moving border frame and lengthy matching between regions. Instead of presenting this, we return to our models and consider surfactant presence without any presumptions on surfactant concentration via no-slip conditions, observing how results differ.

Chapter 6

Surface Viscosity

Complete surfactant modelling demands underlying chemistry and leads to elaborate Marangoni models beyond this essay's scope (see [7]). However, an alternative more suitable than the no-slip condition involves **surface viscosity**: treating the surface as a liquid of different viscosity from the bulk. This offers more simplicity than Marangoni modelling, while no oversimplifications on surfactant concentration as in [20] are needed. Instead, surfactant effects are controlled via a parameter V_s.

A constitutive relation for surface viscosity depends on the surface's rate of strain (see [5] and [11]):

$$\sigma^\star = \eta^\star \frac{\partial u_s^\star}{\partial x^\star}, \tag{6.1}$$

where $u_s^\star$ is the surface velocity and the surface viscosity $\eta^\star$ is assumed constant for simplicity, but varies in literature: $\eta^\star \sim 2 \times 10^{-7}\ \mathrm{kg\,s^{-1}}$ in Dey et al. [11], whereas Bikerman [4] uses $\eta^\star \sim 3 \times 10^{-5}\ \mathrm{kg\,s^{-1}}$. We therefore consider regimes corresponding to different orders of magnitude.

6.1 Configuration

We maintain our $O(1)$, $O(\epsilon^2)$ equations and the assumption $\sigma_+^\star = \sigma_-^\star$, as well as the kinematic condition and normal stress from Chapter 2. However, surfactant presence gives shear stress:

$$\mathbf{t}_\pm \tau \mathbf{n}_\pm = \pm \frac{\partial \sigma^\star}{\partial x^\star}. \tag{6.2}$$

Consequently, (BC2) becomes:

$$\left[\frac{\mu^\star U_0}{\epsilon L_0}\right]\frac{(u_z+\epsilon^2 w_x)(1-\epsilon^2(H_x\pm\frac{1}{2}h_x)^2)+2\epsilon^2(H_x\pm\frac{1}{2}h_x)(w_z-u_x)}{\sqrt{1+\epsilon^2(H_x\pm\frac{1}{2}h_x)^2}}=\pm\left[\frac{\eta^\star U_0}{L_0^2}\right]\frac{\partial^2 u_s}{\partial x^2}. \tag{6.3}$$

Defining the *surface viscosity ratio*:

$$V_s=\frac{\eta^\star}{\epsilon\mu^\star L_0}, \tag{6.4}$$

the above becomes:

$$\pm\epsilon^2 V_s\frac{\partial^2 u_s}{\partial x^2}=\frac{(u_z+\epsilon^2 w_x)(1-\epsilon^2(H_x\pm\frac{1}{2}h_x)^2)+2\epsilon^2(H_x\pm\frac{1}{2}h_x)(w_z-u_x)}{\sqrt{1+\epsilon^2(H_x\pm\frac{1}{2}h_x)^2}}. \tag{6.5}$$

If V_s is sufficiently large, σ-gradients enter at $O(1)$ in (6.5). For "medium" V_s, this occurs at $O(\epsilon^2)$, whereas σ-gradients are negligible when V_s is very small.

6.2 Medium surface viscosity: $V_s \sim O(\epsilon^{-1})$

Suppose V_s is such that the left-hand side of (6.5) enters at $O(\epsilon^2)$. Then, (BC2$O(1)$) from Chapter 2 is unchanged, while (BC2$O(\epsilon^2)$) becomes:

$$\pm V_s\frac{\partial^2 u_s}{\partial x^2}=\frac{\partial u_1}{\partial z}+\frac{\partial w_0}{\partial x}\mp 2\frac{\partial h_0}{\partial x}\frac{\partial u_0}{\partial x}. \tag{6.6}$$

The analysis of Chapter 2 is identical, up until (2.33) when V_s enters at $O(\epsilon^2)$:

$$\left[\frac{\partial u_1}{\partial z}\right]_{z=-\frac{1}{2}h_0}^{z=\frac{1}{2}h_0}-2V_s\frac{\partial^2 u_s}{\partial x^2}=\left[-\frac{\partial w_0}{\partial x}\right]_{z=-\frac{1}{2}h_0}^{z=\frac{1}{2}h_0}+2\frac{\partial h_0}{\partial x}\frac{\partial u_0}{\partial x}+2\frac{\partial h_0}{\partial x}\frac{\partial u_0}{\partial x}=h_0\frac{\partial^2 u_0}{\partial x^2}+4\frac{\partial h_0}{\partial x}\frac{\partial u_0}{\partial x}. \tag{6.7}$$

Note that (2.19) holds, so $u=u(x,t)=u_s=\bar{u}$. Combining (6.7) with (2.32), our equations read:

Thin-film equations (surface viscosity)

$$\frac{\partial h}{\partial t}+\frac{\partial}{\partial x}(uh)=0, \tag{TFE1SV}$$

$$\frac{\partial}{\partial x}\left(4h\frac{\partial u}{\partial x}\right)+2V_s\frac{\partial^2 u}{\partial x^2}+\frac{\epsilon}{2\mathrm{Ca}}h\frac{\partial^3 h}{\partial x^3}=0, \tag{TFE2SV}$$

where $\mathrm{Ca} = \mu^\star U_0/\gamma^\star$ and $\gamma^\star$ is the constant component of surface tension. To proceed, we first consider a configuration where $V_s \sim O(\epsilon^{-1})$, so surface viscosity dominates (L) and we assume capillarity dominates (PB) as before (see Appendix A.3). In the lamella, this makes viscosity negligible, simplifying (TFE1SV)-(TFE2SV) to:

Lamella model ($V_s \sim O(\epsilon^{-1})$)

$$\frac{\partial h}{\partial t} + \frac{\partial}{\partial x}(uh) = 0, \tag{L1SV}$$

$$\frac{\partial^2 u}{\partial x^2} = 0. \tag{L2SV}$$

The accompanying boundary conditions remain (BCL1), (BCL2), and (ICL1).

6.2.1 Lagrangian description

When considering this model, Breward [5] assumes that the lamella remains spatially uniform, but does not explicitly show this. As in Chapter 3, here we show $h(x,0) = 1$ implies $h(x,t) \equiv h_L(t), \forall t \geq 0$. Using Lagrangian coordinates (3.20), (L1SV) becomes:

$$\frac{\partial h}{\partial \tau} + h\frac{\partial^2 x}{\partial X \partial \tau}\left(\frac{\partial x}{\partial X}\right)^{-1} = \left(\frac{\partial x}{\partial X}\right)^{-1}\frac{\partial}{\partial \tau}\Bigg(\underbrace{h\frac{\partial x}{\partial X}}_{P(X)}\Bigg) = 0 \tag{6.8}$$

We integrate (L2SV) once and use the chain rule:

$$G(\tau) = \frac{\partial u}{\partial x} = \frac{\partial^2 x}{\partial X \partial \tau}\left(\frac{\partial x}{\partial X}\right)^{-1} = \frac{\partial}{\partial \tau}\left(\log\left|\frac{\partial x}{\partial X}\right|\right). \tag{6.9}$$

Subsequent integration gives us:

$$\left|\frac{\partial x}{\partial X}\right| = \exp\Big[\tilde{G}(\tau) + R(X)\Big], \tag{6.10}$$

where $\tilde{G}'(\tau) = G(\tau)$ and $\tilde{G}(0) = 0$. Recalling (6.8), we see

$$\frac{\partial x}{\partial X} = \frac{P(X)}{h(X,\tau)}, \tag{6.11}$$

so that $t = \tau = 0$ and $h(x,0) = 1$ in (6.10) give:

$$|P(X)| = \exp\Big[R(X)\Big] \tag{6.12}$$

Finally, plugging this into (6.10):

$$h(x,t) = e^{-\tilde{G}(t)}, \tag{6.13}$$

thus spatial uniformity $h(x,t) = h_L(t)$ follows, so the matching condition (M1) holds.

6.2.2 Transition region

Nondimensionalising as in (3.7), our model is:

$$\frac{\partial h}{\partial t} + \frac{1}{\delta}\frac{\partial}{\partial \xi}(uh) = 0, \tag{6.14}$$

$$\frac{\partial}{\partial \xi}\left(4h\frac{\partial u}{\partial \xi}\right) + 2V_s\frac{\partial^2 u}{\partial \xi^2} + \frac{\epsilon}{2\delta \mathrm{Ca}}h\frac{\partial^3 h}{\partial \xi^3} = 0, \tag{6.15}$$

with matching conditions (M1)-(M3). To balance surface viscosity and capillarity in (6.15), we set:

$$\frac{V_s \mathrm{Ca}\delta}{\epsilon} = 1. \tag{6.16}$$

The definition of Ca determines the velocity scale:

$$U_0 = \frac{\epsilon^2 \gamma^\star L_0}{\delta \eta^\star}. \tag{6.17}$$

At $O(1)$ in δ, as $V_s \sim O(\epsilon^{-1})$, (6.14)-(6.15) become:

$$\frac{\partial}{\partial \xi}(uh) = 0, \tag{6.18}$$

$$2\frac{\partial^2 u}{\partial \xi^2} + \frac{1}{2}h\frac{\partial^3 h}{\partial \xi^3} = 0. \tag{6.19}$$

Integrating (6.18) and appealing to (M2), we see:

$$u(\xi, t)h(\xi, t) = Q(t). \tag{6.20}$$

As in the surfactant-free case, integrating (6.19) using $\frac{\partial}{\partial \xi}(hh_{\xi\xi} - \frac{1}{2}h_\xi^2) = hh_{\xi\xi\xi}$ yields:

$$2\frac{\partial u}{\partial \xi} + \frac{1}{2}h\frac{\partial^2 h}{\partial \xi^2} - \frac{1}{4}\left(\frac{\partial h}{\partial \xi}\right)^2 = A(t) = 0, \tag{6.21}$$

where the last equality comes from (M1). Multiplying by $h^{-3/2}$ and eliminating u via (6.20), then integrating, we see:

$$\frac{8Q}{5h^2} + \frac{\partial h}{\partial \xi} = B(t)\sqrt{h}. \tag{6.22}$$

As before, matching (T) with (PB) gives different results for semi-dry and dry foams.

6.2.2.1 Semi-dry foam

When the curvature radius is constant, (M3) gives $B(t) = \sqrt{2}$. Taking $\xi \to -\infty$, we finally use (M2) to obtain:

$$Q(t) = \frac{5\sqrt{2}h_L^{\frac{5}{2}}}{8}. \tag{6.23}$$

Then, we integrate (L2SV) twice, using the spatially uniform (BCL1) and (BCL2) to obtain:

$$u(x,t) = \frac{5\sqrt{2}h_L^{\frac{3}{2}}(t)}{8}x. \tag{6.24}$$

Substituting (6.24) into (L1SV), we get an ODE for h_L:

$$\frac{dh_L}{dt} = -\frac{5\sqrt{2}h_L^{\frac{5}{2}}}{8}. \tag{6.25}$$

We solve this by separating variables, recalling $h_L(0) = 1$ to see:

$$\frac{2}{3}\frac{1}{h_L\sqrt{h_L}} = \frac{5\sqrt{2}}{8}t + \frac{2}{3}. \tag{6.26}$$

Rearranging, we obtain:

Breward & Howell $V_s \sim O(\epsilon^{-1})$ thinning

$$h_L(t) = \frac{1}{\left(\frac{15\sqrt{2}}{16}t + 1\right)^{\frac{2}{3}}}. \tag{6.27}$$

Rupture times for various configurations are calculated in Appendix A.

6.2.2.2 Dry foam

As in Chapter 4, we reconcile curvature changes using:

$$\frac{\partial^2 h}{\partial \xi^2} \to \frac{1}{a(t)} \text{ as } \xi \to \infty. \tag{M3'}$$

Previous calculations until (6.22) still hold, after which (M3') gives $B(t) = \sqrt{\frac{2}{a(t)}}$. Letting $\xi \to -\infty$ in (6.22), the flux becomes:

$$Q(t) = \frac{5\sqrt{2}}{8}\frac{h_L^{\frac{5}{2}}}{a^{\frac{1}{2}}}. \tag{6.28}$$

Written in dry foam variables $(\tilde{t}, \tilde{h})$ from Chapter 4, our ODE reads:

$$\frac{d\tilde{h}_L}{d\tilde{t}} = -\frac{10(1+\tilde{\omega})}{3}\tilde{h}_L^{\frac{5}{2}}(1-\tilde{h}_L)^{-\frac{1}{4}}, \tag{6.29}$$

with initial condition:

$$\tilde{h}_L(0) = \frac{1}{1+\tilde{\omega}}. \tag{6.30}$$

We may again express the solution using Gauss' hypergeometric function (compare with (4.31)):

Brush & Davis $V_s \sim O(\epsilon^{-1})$ thinning

$$\frac{10(1+\tilde{\omega})\tilde{t}}{3} = \frac{2(1-\tilde{h}_L)^{\frac{1}{4}}(2-\tilde{h}_L) + \tilde{h}_L^2 F(\frac{1}{2},\frac{3}{4},\frac{3}{2};\tilde{h})}{6\tilde{h}_L^{\frac{3}{2}}} + \frac{2(1-\tilde{h}_L(0))^{\frac{1}{4}}(2-\tilde{h}_L(0)) + \tilde{h}_L(0)^2 F(\frac{1}{2},\frac{3}{4},\frac{3}{2};\tilde{h}_L(0))}{6\tilde{h}_L(0)^{\frac{3}{2}}}. \tag{6.31}$$

To compare all regimes, we convert (6.25) to $(\tilde{t}, \tilde{h})$ coordinates, obtaining:

$$\frac{d\tilde{h}_L}{d\tilde{t}} = -\frac{10}{3}(1+\tilde{\omega})^{\frac{5}{4}}\tilde{\omega}^{-\frac{1}{4}}\tilde{h}_L^{\frac{5}{2}}. \tag{6.32}$$

We summarise all models and give log-log plots:

Comparison of all models: surface viscosity in dry/semi-dry foams		
Model	V_s	Governing ODE
Breward & Howell ($\frac{a_0}{L_0} \sim O(1)$)	$V_s << 1$	$\frac{d\tilde{h}_L}{d\tilde{t}} = -\frac{(1+\tilde{\omega})^{\frac{1}{4}}}{\omega^{\frac{1}{4}}}\tilde{h}_L^{\frac{3}{2}}$
Breward & Howell ($\frac{a_0}{L_0} \sim O(1)$)	$V_s \sim O(\epsilon^{-1})$	$\frac{d\tilde{h}_L}{d\tilde{t}} = -\frac{10}{3}(1+\tilde{\omega})^{\frac{5}{4}}\tilde{\omega}^{-\frac{1}{4}}\tilde{h}_L^{\frac{5}{2}}$
Brush & Davis ($\frac{L_0 h_0}{a_0^2} \sim O(1)$)	$V_s << 1$	$\frac{d\tilde{h}_L}{d\tilde{t}} = -\tilde{h}_L^{\frac{3}{2}}(1-\tilde{h}_L)^{-\frac{1}{4}}$
Brush & Davis ($\frac{L_0 h_0}{a_0^2} \sim O(1)$)	$V_s \sim O(\epsilon^{-1})$	$\frac{d\tilde{h}_L}{d\tilde{t}} = -\frac{10(1+\tilde{\omega})}{3}\tilde{h}_L^{\frac{5}{2}}(1-\tilde{h}_L)^{-\frac{1}{4}}$

From Figure 6.1, the relationship between dry and semi-dry foams in the presence of surfactants is very similar to the surfactant-free case, with dry foam exhibiting larger $\tilde{t}$ for each fixed $\tilde{h}$. However, for typical bubbles as in Appendix A.2, the velocity scaling (6.17) will be much larger for dry foams, due to the decrease in δ caused by a_0. In turn, this accelerated flux leads to the paradox of dry foams rupturing first,

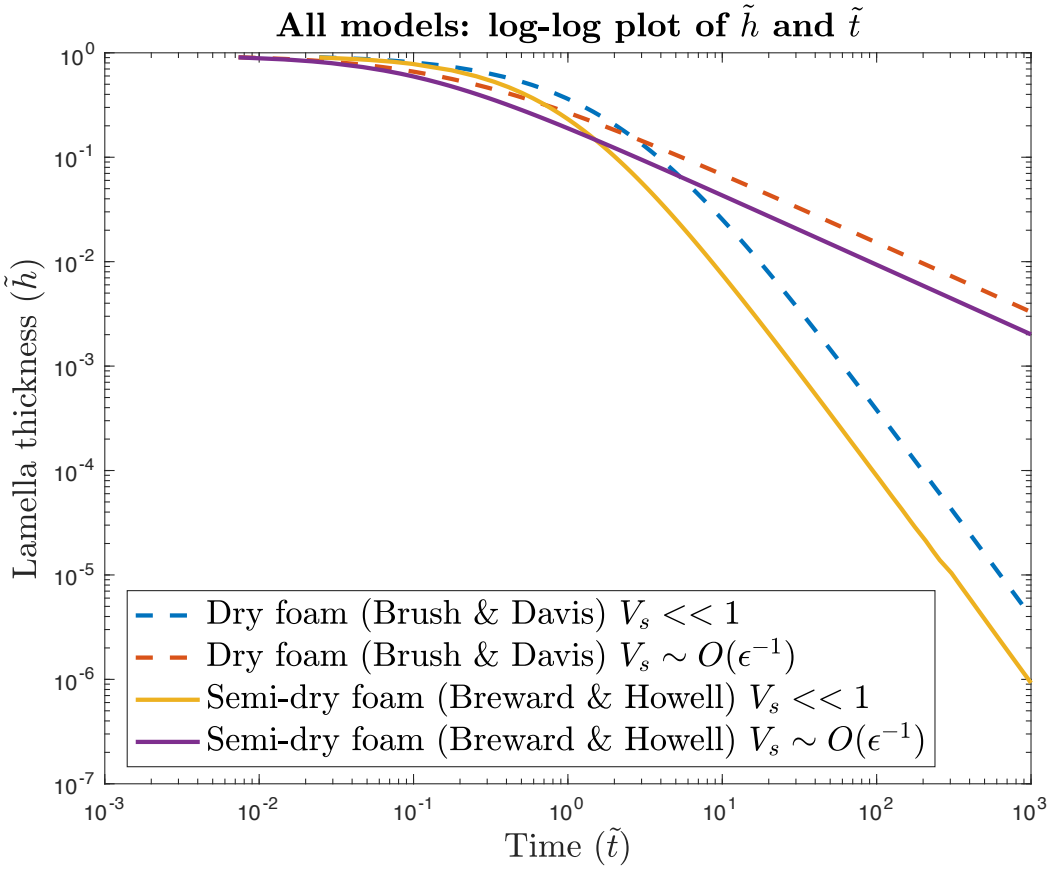

Figure 6.1: $V_s \sim O(\epsilon^{-1})$ and $V_s \ll 1$ regimes.

despite the visual suggestion of the non-dimensional plot. Overall, we observe that the rate of thinning is much slower for foams stabilised by $V_s \sim O(\epsilon^{-1})$ (see Appendix A.3 for calculations).

6.3 Low surface viscosity: $V_s \sim O(1)$

We consider instead $V_s \sim O(1)$, so viscosity in (TFE2SV) is non-negligible. In (T), all effects balance, so (6.19) is replaced with:

$$\frac{\partial}{\partial \xi}\left(4h\frac{\partial u}{\partial \xi}\right) + 2V_s\frac{\partial^2 u}{\partial \xi^2} + \frac{\epsilon}{2\delta \mathrm{Ca}}h\frac{\partial^3 h}{\partial \xi^3} = 0. \tag{6.33}$$

In the regime where $V_s \mathrm{Ca}\delta/\epsilon = 1$ for the second and third terms to balance, as in all previous cases we integrate this once to obtain:

$$-\frac{8Q}{h}\frac{\partial h}{\partial \xi} - \frac{4V_s}{h^2}\frac{\partial h}{\partial \xi} + V_s h^{\frac{3}{2}}\frac{\partial}{\partial \xi}\left(\frac{1}{\sqrt{h}}\frac{\partial h}{\partial \xi}\right) = C(t). \tag{6.34}$$

Determining $C(t)$ requires (M1), which relies on spatial uniformity of $h(x,t)$. A Lagrangian coordinate argument would not succeed here; instead we *assume* $h(x,t) = h_L(t)$ to apply (M1). Then, $C(t) = 0$ and another integration gives:

$$\frac{16Q}{3V_s h^{\frac{3}{2}}} + \frac{8Q}{5h^{\frac{5}{2}}} + \frac{1}{\sqrt{h}}\frac{\partial h}{\partial \xi} = D(t), \tag{6.35}$$

where (M3) tells us $D(t) = \sqrt{2}$ for semi-dry foams and (M3') gives $D(t) = \sqrt{\frac{2}{a(t)}}$ for dry foams. Using (M1), we obtain:

$$Q_{semi-dry} = \frac{\sqrt{2}}{\frac{16}{3V_s h_L^{\frac{3}{2}}} + \frac{8}{5h_L^{\frac{5}{2}}}}, \tag{6.36}$$

$$Q_{dry} = \frac{\sqrt{\frac{2}{a(t)}}}{\frac{16}{3V_s h_L^{\frac{3}{2}}} + \frac{8}{5h_L^{\frac{5}{2}}}}. \tag{6.37}$$

Before solving the resulting equations numerically, we convert to $(\tilde{t}, \tilde{h})$ coordinates. For (6.36) we obtain:

$$\frac{d\tilde{h}_L}{d\tilde{t}} = -\frac{\omega^{-\frac{1}{4}}}{\frac{1}{V_s \tilde{h}_L^{\frac{3}{2}}(1+\tilde{\omega})^{\frac{1}{4}}} + \frac{3}{10\tilde{h}_L^{\frac{5}{2}}(1+\tilde{\omega})^{\frac{5}{4}}}}, \tag{6.38}$$

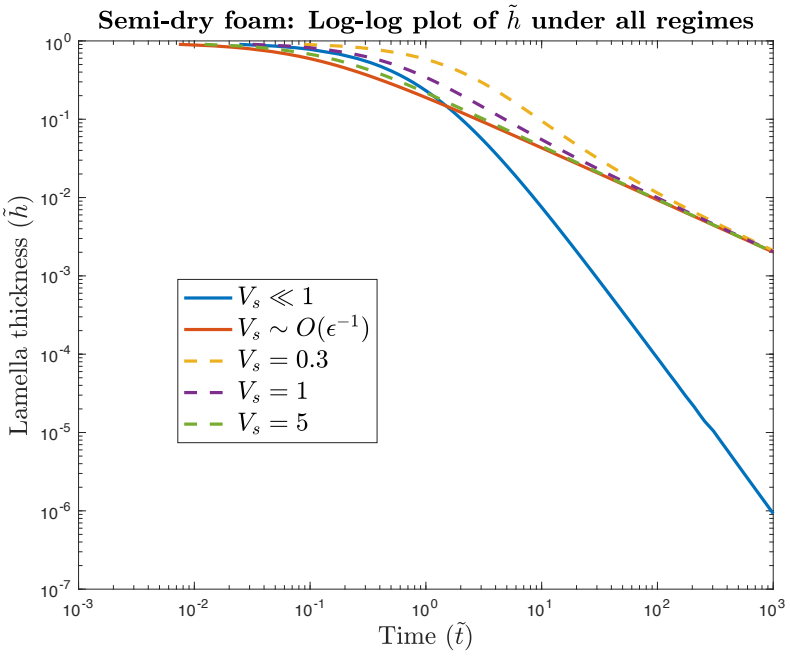

Figure 6.2: Semi-dry foam thinning for five values of V_s.

whereas (6.37) becomes:

$$\frac{d\tilde{h}_L}{d\tilde{t}} = -\frac{(1-\tilde{h}_L)^{-\frac{1}{4}}}{\dfrac{1}{V_s\tilde{h}_L^{\frac{3}{2}}} + \dfrac{3}{10\tilde{h}_L^{\frac{5}{2}}(1+\tilde{\omega})}}. \tag{6.39}$$

We may then plot these regimes alongside the previous configurations.

In Figures 6.2 and 6.3, we observe the same behaviour for each type of foam. Namely, when $V_s \sim O(1)$ but is relatively small ($V_s = 0.3$), viscous contributions in (6.36)-(6.37) are noticeable and initial thinning is similar to $V_s \ll 1$. However, as V_s increases ($V_s = 5$), the curves get closer to the $V_s \sim O(\epsilon^{-1})$ case. Later on, surface viscosity dominates, with all $V_s \sim O(1)$ regimes converging to the $V_s \sim O(\epsilon^{-1})$ curve. This is unsurprising: since $V_s \sim O(\epsilon^{-1})$ leads roughly to a $\tilde{t}^{-\frac{2}{3}}$ law, whereas $V_s \ll 1$ gives $\tilde{t}^{-2}$ behaviour, as $\tilde{t} \to \infty$ the former dominates in the composite fluxes (6.36)-(6.37). This implies an interesting conclusion: the lower the critical thickness ($\tilde{h} < 10^{-2}$ in our plots) and hence the greater $\tilde{t}$ until rupture, the more justified it is to ignore viscous effects in (TFE2SV) even if V_s is small. Of course, this does not imply rupture times are independent of V_s: redimensionalising time using (2.9) and (6.17) shows that all else equal, higher V_s (therefore higher $\eta^\star$) leads to slower thinning, as anticipated.

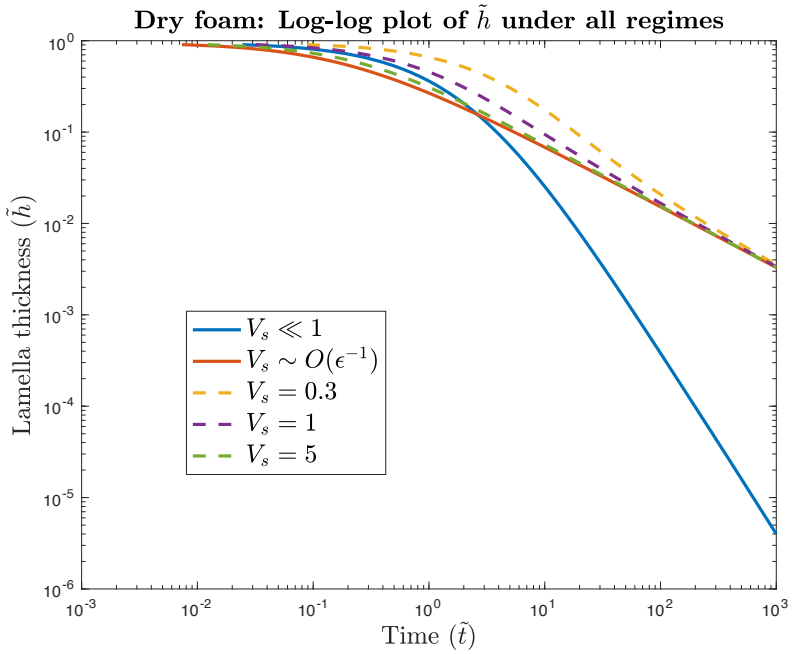

Figure 6.3: Dry foam thinning for same V_s as in Figure 6.2.

6.4 High surface viscosity $V_s \sim O(\epsilon^{-2})$

So far, we have treated $V_s \sim O(\epsilon^{-1})$ and $V_s \sim O(1)$, with $\mathrm{Ca} \sim O(\epsilon)$. If surface viscosity is more dominant, say $V_s \sim O(\epsilon^{-2})$, then σ-gradients enter (6.5) at $O(1)$. Following Breward [5], we consider a regime where capillary, lubrication, and surface viscous effects all matter: this requires $\mathrm{Ca} \sim O(\epsilon^3)$ and rescaling $p \to \frac{p}{\epsilon^2}$ for non-trivial balances, exactly as in Schwartz & Princen's no-slip model. The asymptotic analysis of Chapter 2 gives the same result as (5.11)-(5.13):

Governing equations $O(1)$

$$\frac{\partial u}{\partial x} + \frac{\partial w}{\partial z} = 0, \tag{6.40}$$

$$\frac{\partial^2 u}{\partial z^2} = \frac{\partial p}{\partial x}, \tag{6.41}$$

$$\frac{\partial p}{\partial z} = 0. \tag{6.42}$$

Furthermore, conditions on $z = H \pm \frac{1}{2}h$ become:

$$\frac{\epsilon^3}{\mathrm{Ca}}\left(\pm \frac{\partial^2 H}{\partial x^2} + \frac{1}{2}\frac{\partial^2 h}{\partial x^2} \right) = -p, \tag{6.43}$$

$$\pm\epsilon^2 V_s \frac{\partial^2 u_s}{\partial x^2} = \frac{\partial u_s}{\partial z}, \tag{6.44}$$

$$w = \frac{\partial H}{\partial t} \pm \frac{1}{2}\frac{\partial h}{\partial t} + u_s\left(\frac{\partial H}{\partial x} \pm \frac{1}{2}\frac{\partial h}{\partial x}\right). \tag{6.45}$$

6.4.1 Reduction to TFEs

From (6.42), $p = p(x,t)$, which allows equating (6.43) from each surface. This gives $H_{xx} = 0$ and by rotating coordinates, $H \equiv 0$.

By integrating as in Schwartz & Princen's model, conservation of mass follows:

$$\frac{\partial h}{\partial t} + \frac{\partial}{\partial x}(\bar{u}h) = 0, \tag{6.46}$$

where:

$$\bar{u} = \frac{1}{h}\int_{-\frac{h}{2}}^{\frac{h}{2}} u(x,z,t)dz. \tag{6.47}$$

Moreover, (6.43) enables us to integrate (6.41) twice:

$$u = -\frac{\epsilon^3}{4\mathrm{Ca}}\frac{\partial^3 h}{\partial x^3}z^2 + E(x,t)z + F(x,t). \tag{6.48}$$

We determine $E(x,t) = 0$ through (6.44), while integrating (6.48) between $-\frac{h}{2}$ and $\frac{h}{2}$ gives:

$$u(x,z,t) = \bar{u} + \frac{\epsilon^3}{4\mathrm{Ca}}\frac{\partial^3 h}{\partial x^3}\left(\frac{h^2}{12} - z^2\right). \tag{6.49}$$

Hence, the flow is parabolic due to increased surface forces, with u_s given by:

$$u_s = \bar{u} - \frac{\epsilon^3}{24\mathrm{Ca}}h^2\frac{\partial^3 h}{\partial x^3}, \tag{6.50}$$

As $u_s \neq 0$ in general, we do not observe no-slip behaviour as in Schwartz & Princen's model.

Finally, we substitute (6.50) into the longitudinal force (6.44):

$$2V_s\frac{\partial^2 \bar{u}}{\partial x^2} - \frac{V_s\epsilon^3}{12\mathrm{Ca}}\frac{\partial^2}{\partial x^2}\left(h^2\frac{\partial^3 h}{\partial x^3}\right) + \frac{\epsilon}{2\mathrm{Ca}}h\frac{\partial^3 h}{\partial x^3} = 0. \tag{6.51}$$

Altogether, our governing equations read:

TFEs ($V_s \sim O(\epsilon^{-2})$)

$$\frac{\partial h}{\partial t} + \frac{\partial}{\partial x}(\bar{u}h) = 0, \tag{6.52}$$

$$2V_s\frac{\partial^2 \bar{u}}{\partial x^2} - \frac{V_s\epsilon^3}{12\mathrm{Ca}}\frac{\partial^2}{\partial x^2}\left(h^2\frac{\partial^3 h}{\partial x^3}\right) + \frac{\epsilon}{2\mathrm{Ca}}h\frac{\partial^3 h}{\partial x^3} = 0. \tag{6.53}$$

6.4.2 Transition region

In (T), (6.52)-(6.53) reduce to:

$$\frac{\partial h}{\partial t} + \frac{1}{\delta}\frac{\partial}{\partial \xi}\left(\bar{u}h\right) = 0, \tag{6.54}$$

$$\frac{2V_s}{\delta^2}\frac{\partial^2 u_s}{\partial \xi^2} + \frac{\epsilon}{2\mathrm{Ca}\delta^3}h\frac{\partial^3 h}{\partial \xi^3} = 0. \tag{6.55}$$

To balance surface viscosity and capillarity, as before we set:

$$V_s = \frac{\epsilon}{\delta \mathrm{Ca}}. \tag{6.56}$$

Next, we define:

$$\beta = \frac{\epsilon^3}{24\mathrm{Ca}\delta^3} = \frac{\epsilon^2}{24\delta^2}V_s, \tag{6.57}$$

which simplifies the expansion of (6.55) via (6.50) to:

$$\frac{\partial^2 \bar{u}}{\partial \xi^2} - \beta\frac{\partial^2}{\partial \xi^2}\left(h^2\frac{\partial^3 h}{\partial \xi^3}\right) + \frac{1}{4}h\frac{\partial^3 h}{\partial \xi^3} = 0. \tag{6.58}$$

As in Section 6.3, we make the assumption that the lamella remains spatially uniform in order to apply (M1). This allows integrating (6.58) much like before:

$$\frac{\partial \bar{u}}{\partial \xi} - \beta\frac{\partial}{\partial \xi}\left(h^2\frac{\partial^3 h}{\partial \xi^3}\right) + \frac{1}{4}h\frac{\partial^2 h}{\partial \xi^2} - \frac{1}{8}\left(\frac{\partial h}{\partial \xi}\right)^2 = 0, \tag{6.59}$$

which after eliminating $\bar{u}$ and by integrating (6.54) at leading order in δ gives:

$$-Q(t)\frac{\partial h}{\partial \xi} - 2\beta h^3\frac{\partial h}{\partial \xi}\frac{\partial^3 h}{\partial \xi^3} - \beta h^4\frac{\partial^4 h}{\partial \xi^4} + \frac{1}{4}h^3\frac{\partial^2 h}{\partial \xi^2} - \frac{1}{8}h^2\left(\frac{\partial h}{\partial \xi}\right)^2 = 0. \tag{6.60}$$

6.4.3 Linear stability analysis

No further integration is possible. Instead, we investigate the well-posedness of the problem by perturbing about limiting behaviours. Starting at $-\infty$, for $c \ll 1$, we write:

$$h \sim h_L(t)\left[1 + ce^{\lambda\xi}\right] \text{ as } \xi \to -\infty. \tag{6.61}$$

Conducting a linear stability analysis (dropping $O(c^2)$ terms) and taking $\xi \to -\infty$, one obtains:

$$\lambda\left[4\beta h_L^4\lambda^3 - h_L^3\lambda + 4Q(t)\right] = 0. \tag{6.62}$$

$\lambda = 0$ is clearly a root, and we are left with $f(\lambda) = \lambda^3 - A\lambda + B = 0$, where:

$$A = \frac{1}{4\beta h_L} > 0, B = \frac{Q(t)}{\beta h_L^4} > 0, \tag{6.63}$$

since we expect $Q(t) > 0$. But since $f(0) = B > 0$ whereas $f(\lambda) \to -\infty$ as $\lambda \to -\infty$, by continuity of $f(\lambda)$ a negative root λ_- always exists. We consider the remaining roots λ_1 and λ_2. The cubic has discriminant $\Delta = 4A^3 - 27B^2$ and two cases arise:

- **Case 1**: $\Delta < 0 \iff 12\sqrt{3\beta}Q > h_L^{\frac{5}{2}}$. Then λ_1, λ_2 are complex conjugates. By Vieta's formulae, since $\lambda_- + \lambda_1 + \lambda_2 = 0$, we see $\Re(\lambda_1) = \Re(\lambda_2) > 0$. These roots correspond to oscillatory decay.
- **Case 2**: $\Delta \geq 0 \iff 12\sqrt{3\beta}Q \leq h_L^{\frac{5}{2}}$. Then $\lambda_1, \lambda_2 \in \mathbb{R}$, equal if and only if $\Delta = 0$. As before $\lambda_1 + \lambda_2 > 0$, and moreover $\lambda_1\lambda_2\lambda_- = -B < 0$. Thus λ_1, λ_2 are both positive, giving monotonic decay as $\xi \to -\infty$.

Consequently, in either case we suppress one growing mode, given by $\lambda = \lambda_- < 0$.

We analyse behaviour as $\xi \to \infty$, by expanding about $h \sim a_1\xi^2/2$. This gives $a_1 = 1$ for semi-dry foam and $a_1 = 1/a(t)$ for dry foam. We write an ansatz:

$$h \sim \frac{a_1\xi^2}{2} + a_2\xi + a_3 + \frac{a_4}{\xi} + \frac{a_5}{\xi^2} + O\left(\frac{1}{\xi^3}\right), \tag{6.64}$$

and substitute it into (6.60) to compare coefficients:

$$O(\xi^5) : -\frac{1}{4}\left(\frac{a_1}{2}\right)^2 a_1 a_2 = 0. \tag{6.65}$$

As $a_1 \neq 0$, it follows that $a_2 = 0$. Similarly:

$$O(\xi^4) : \frac{3}{4}\left(\frac{a_1}{2}\right)^2 a_3 a_1 - \frac{1}{8}a_1 a_3 a_1^2 = 0, \tag{6.66}$$

so $a_3 = 0$ as well. At further others the algebra gets more complicated:

$$O(\xi^3) : 12\beta\left(\frac{a_1}{2}\right)^3 a_1 a_4 - 24\beta\left(\frac{a_1}{2}\right)^4 a_4 + \frac{1}{4}\left(\frac{a_1}{2}\right)^3 a_4 + \frac{1}{4}\left(\frac{a_1}{2}\right)^2 a_1 a_4 = 0, \tag{6.67}$$

therefore $a_4 = 0$. Consequently, the ansatz (6.64) is an oversimplification, and almost certainly logarithmic terms need to be introduced. This system could undergo numerical simulations, however, it is as complicated as more complete Marangoni models (see [7]). Treating it in more detail is therefore of little significance.

Chapter 7

Conclusion

In this essay, we followed the derivation of a sophisticated model of foam stability, due to Breward & Howell [7], starting from the Navier-Stokes equations and appropriate boundary conditions. Afterwards, we considered a work by Brush & Davis [8], which challenges a central assumption on constant curvature, thereby inducing a new configuration where the initial model was applicable with a modification. The final chapter presented numerous original results: by building upon "medium" surface viscosity as studied by Breward [5], we utilised an approach by Howell [13] to confirm an assumption on spatial uniformity of lamellae. We also managed to frame this notion of surface viscosity within the "dry" limit of Brush & Davis' model. Moreover, we presented a new regime of "low" surface viscosity, where we resorted to numerical solutions and explained resulting behaviour in relation to other regimes. Finally, we conducted a partial linear stability analysis for "high" surface viscosity; we were unable to obtain a numerical or analytic solution, but we drew parallels to Schwartz & Princen's work [20], which predicted parabolic velocity when surfactants dominate.

Many avenues for further exploration may be taken. It would be insightful to investigate these models using van der Waals intermolecular forces instead of replace critical thicknesses. This has been done for films bounded by a solid surface by Ruckenstein & Jain [18], while a bifurcation analysis for free-films was conducted by Erneux & Davis [12]. Further, repeating the surface viscosity analysis for non-negligible inertia would resolve limiting cases when Re becomes large, as occasionally observed for water and aluminum (see [8]). Ultimately, the configurations presented here represent the frontier of analytic solutions, and any improvement in modelling requires both sophisticated chemistry and advanced numerical computations.

Appendix A

Parameter Sizes

A.1 Surfactant-free bubbles

We consider a typical bubble with:

$$\epsilon \sim 10^{-3},\ L_0 \sim 10^{-3}\text{m},\ a_0 \sim 4\times 10^{-4}\text{m}. \tag{A.1}$$

This gives the transition region rescaling:

$$\delta = \sqrt{\frac{\epsilon a_0}{2L_0}} \approx 0.014 \ll 1. \tag{A.2}$$

Importantly, the aspect ratio of (T), $\text{Ca} = \epsilon/\delta \approx 0.07$, is still small. As $\epsilon/\text{Ca} \ll 1$, the corresponding term in (TFE2) in Chapter 3 renders capillary effects negligible in the lamella.

For water, typical values are:

$$\mu^\star = 10^{-3}\text{Kgm}^{-1}\text{s}^{-1}, \tag{A.3}$$

$$\sigma^\star = 7\times 10^{-2}\text{Nm}^{-1}. \tag{A.4}$$

We recall (3.51) for semi-dry foams:

$$t_c^\star = \frac{16\mu^\star L_0\sqrt{a_0}}{3\sigma^\star}\left[\frac{1}{\sqrt{h_c^\star}} - \frac{1}{\sqrt{h_0}}\right]. \tag{A.5}$$

The above parameters give $t_c^\star \approx 3\times 10^{-3}$s if $h_c = 0.1h_0$ and $t_c^\star \approx 1.4\times 10^{-2}$s if $h_c = 0.01h_0$.

A.2 Semi-dry versus dry foam paradox

We take typical values as in Brush & Davis [8]

$$h_0 = 10^{-7}\text{m}, L_0 = 10^{-3}\text{m}, a_0^{semi-dry} = 10^{-3}\text{m}, a_0^{dry} = 10^{-5}\text{m}, \tag{A.6}$$

so that $\sqrt{L_0 h_0}/a_0^{dry} = 1$ as in our plots. For semi-dry foam, we find:

$$U_0^{semi-dry} = \frac{\sigma^\star}{\mu^\star}\sqrt{\frac{2h_0}{a_0^{semi-dry}}} \approx 0.99\text{ms}^{-1}, \tag{A.7}$$

whereas for dry foams:

$$U_0^{dry} = \frac{\sigma^\star}{\mu^\star}\sqrt{\frac{2h_0}{a_0^{dry}}} = 10U_0^{semi-dry} \approx 9.9\text{ms}^{-1} \tag{A.8}$$

For fixed $\tilde{h}_c$, we see from Figure 4.5 that:

$$1 < \frac{\tilde{t}_c^{dry}}{\tilde{t}_c^{semi-dry}} < 10 \tag{A.9}$$

So rescaling $\tilde{t}$ to t, then nondimensionalising $t^\star/t = L_0/U_0$, by (A.7)-(A.8), dry lamellae rupture quicker, even though the nondimensional time suggests otherwise.

A.3 Bubbles with $V_s \sim O(\epsilon^{-1})$

For semi-dry foam under $V_s \sim O(\epsilon^{-1})$:

$$U_0 = \frac{\epsilon^2 \gamma^\star L_0}{\delta \eta^\star}. \tag{A.10}$$

Using the values from A.1:

$$\text{Ca} = \frac{\mu^\star \epsilon^2 L_0}{\delta \eta^\star} \approx 3.6 \times 10^{-4}. \tag{A.11}$$

As $\text{Ca} \ll 1$ and $\epsilon/V_s\text{Ca} \ll 1$, surface viscosity dominates (L) and capillarity dominates (PB), as assumed earlier. For the rupture time, from (6.27) we have:

$$t_c = \frac{16}{5\sqrt{2}}\left[\frac{1}{h^{\frac{3}{2}}} - 1\right]. \tag{A.12}$$

Redimensionalising using (2.9) and (6.17), this becomes:

$$t_c^\star = \frac{8\eta^\star L_0\sqrt{a_0}}{15\gamma^\star}\left[\left(\frac{1}{h_c^\star}\right)^{\frac{3}{2}} - \left(\frac{1}{h_0}\right)^{\frac{3}{2}}\right]. \tag{A.13}$$

Taking $\eta^\star = 2 \times 10^{-7}\text{kg s}^{-1}$, $\gamma^\star = 7 \times 10^{-2}\text{Nm}^{-1}$ gives rupture times $t_c^\star \approx 0.933s$ and $t_c^\star \approx 30.45s$ for $h_c = 0.1h_0$ and $h_c = 0.01h_0$, respectively, significantly longer than corresponding surfactant-free drainage in A.1.

Appendix B

MATLAB Code for Numerical Solutions

Listing B.1: Code for Figure 3.5

```
tspan = [-7 3]; % the range of xi over which we will solve
    the ODE

h0 = 1.000001 % specify (M1) as the condition as xi
   becomes small
% we want h0 to be close to (but not equal to 1)

% here t takes the role of xi
% solving numerically the ODE for the transition region
   profile
[t,h] = ode45(@(t,h) sqrt(2)*(h^(1/2)-h^(-1)), tspan, h0);

graph1 = plot(t,h)
set(graph1,'LineWidth',2)

% set the axes to their usual origins
ax = gca;
ax.XAxisLocation = 'origin';
ax.YAxisLocation = 'origin';

title('\textbf{Shape of (T) in terms of rescaled variables
    $\hat{h}, \hat{\xi}$}','Interpreter', 'latex','
   fontsize',16)
xlabel('Transition region length ($\hat{\xi}$)', '
   Interpreter', 'latex', 'fontweight','bold','fontsize'
   ,16);
```

```
ylabel('Lamellar thickness ($\hat{h}$)', 'Interpreter', '
    latex','fontweight','bold','fontsize',16);
```

Listing B.2: Code for Figure 4.4

```
tspan = [0 1000]; % the range of t over which we will
    solve the ODEs
w = tan(pi/6) - pi/6 % defining our omega
h0 = 1/(1+w); % setting the initial condition for the ODE

% ODE for dry foam (no surface viscosity)
[t,h] = ode45(@(t,h) -h^(3/2)*(1-h)^(-1/4), tspan, h0);
graph1 = loglog(t,h,'--') % log-log plot, dashed line
set(graph1,'LineWidth',2)
hold on

a = ((1+w)/w)^(1/2)*(1-h).^(1/2) % curvature radius
graph2 = loglog(t,a)
set(graph2,'LineWidth',2)

title('\textbf{Log-log plot of $\tilde{h}$ and $\tilde{a}$
    for dry foam}','Interpreter', 'latex','fontsize',16)
xlabel('Time ($\tilde{t}$)', 'Interpreter', 'latex', '
    fontweight','bold','fontsize',16);
ylabel('Lamella thickness ($\tilde{h}$)', 'Interpreter', '
    latex','fontweight','bold','fontsize',16);
legend({'Dry foam thickness $\tilde{h}$','Radius of
    curvature $\tilde{a}$'}, 'FontSize',16,'Interpreter', '
    latex')
hold off
```

Listing B.3: Code for Figure 4.5

```
w = tan(pi/6) - pi/6 % defining our omega
tspan = [0 100]; % the range of t over which we will solve
    the ODE

% First solve the ODE for dry foam
h0 = 1/(1+w); % setting the initial condition for the ODE
[t,h] = ode45(@(t,h) -h^(3/2)*(1-h)^(-1/4), tspan, h0);
graph1 = loglog(t,h,'--') % log-log plot, dashed line
set(graph1,'LineWidth',2)
hold on

% Now solve the ODE for semi-dry foam
[t,h] = ode45(@(t,h) -h^(3/2)*((1+w)/w)^(1/4), tspan, h0);
graph2 = loglog(t,h) % log-log plot, solid line
```

```
set(graph2,'LineWidth',2)

title('\textbf{Log-log plot of dry versus semi-dry foam
   thinning laws}','Interpreter', 'latex', 'fontweight','
   bold','fontsize',16)
xlabel('Time ($\tilde{t}$)', 'Interpreter', 'latex', '
   fontweight','bold','fontsize',16);
ylabel('Lamella thickness ($\tilde{h}$)', 'Interpreter', '
   latex','fontweight','bold','fontsize',16);
legend({'Brush & Davis (Dry)','Breward & Howell (Semi-Dry)
   '}, 'FontSize',16)
hold off
```

Listing B.4: Code for Figure 6.1

```
tspan = [0 1000]; % the range of t over which we will
   solve the ODEs
w = tan(pi/6) - pi/6 % defining our omega
h0 = 1/(1+w); % setting the initial condition for the ODE

% ODE for dry foam, no surface viscosity
[t,h] = ode45(@(t,h) -h^(3/2)*(1-h)^(-1/4), tspan, h0);
graph1 = loglog(t,h,'--') % log-log plot, dashed line
set(graph1,'LineWidth',2)
hold on

% ODE for dry foam, medium surface viscosity
[t,h] = ode45(@(t,h) -10/3*(1+w)*h^(5/2)*(1-h)^(-1/4),
   tspan, h0);
graph2 = loglog(t,h,'--') % log-log plot, dashed line
set(graph2,'LineWidth',2)

% ODE for semi-dry foam, no surface viscosity
[t,h] = ode45(@(t,h) -h^(3/2)*((1+w)/w)^(1/4), tspan, h0);
graph3 = loglog(t,h) % log-log plot, solid line
set(graph3,'LineWidth',2)

% ODE for semi-dry foam, medium surface viscosity
[t,h] = ode45(@(t,h) -10/3*(1+w)^(5/4)*w^(-1/4)*h^(5/2),
   tspan, h0);
graph4 = loglog(t,h) % log-log plot, solid line
set(graph4,'LineWidth',2)

title('\textbf{All models: log-log plot of $\tilde{h}$ and
    $\tilde{t}$}','Interpreter', 'latex','fontsize',16)
xlabel('Time ($\tilde{t}$)', 'Interpreter', 'latex', '
```

```
   fontweight','bold','fontsize',16);
ylabel('Lamella thickness ($\tilde{h}$)', 'Interpreter', '
   latex','fontweight','bold','fontsize',16);
legend({'Dry foam (Brush \& Davis) $V_s << 1$','Dry foam (
   Brush \& Davis) $V_s \sim O(\epsilon^{-1})$', 'Semi-dry
    foam (Breward \& Howell) $V_s << 1$', 'Semi-dry foam (
   Breward \& Howell) $V_s \sim O(\epsilon^{-1})$'}, '
   FontSize',16,'Interpreter', 'latex')
hold off
```

Listing B.5: Code for Figure 6.2

```
tspan = [0 1000]; % the range of t over which we will
   solve the ODEs
w = tan(pi/6) - pi/6 % defining our omega
h0 = 1/(1+w); % setting the initial condition for the ODE

% ODE for semi-dry foam, no surface viscosity
[t,h] = ode45(@(t,h) -h^(3/2)*((1+w)/w)^(1/4), tspan, h0);
graph1 = loglog(t,h) % log-log plot, solid line
set(graph1,'LineWidth',2)
hold on

% ODE for semi-dry foam, medium surface viscosity
[t,h] = ode45(@(t,h) -10/3*(1+w)^(5/4)*w^(-1/4)*h^(5/2),
   tspan, h0);
graph2 = loglog(t,h) % log-log plot, solid line
set(graph2,'LineWidth',2)

% ODE for semi-dry foam, V_s = 0.3
[t,h] = ode45(@(t,h) -w^(-1/4)/(1/(0.3*h^(3/2)*(1+w)^(1/4)
   )+ 3/(10*h^(5/2)*(1+w)^(5/4))), tspan, h0);
graph3 = loglog(t,h,'--') % log-log plot, dashed line
set(graph3,'LineWidth',2)

% ODE for semi-dry foam, V_s = 1
[t,h] = ode45(@(t,h) -w^(-1/4)/(1/(h^(3/2)*(1+w)^(1/4))+
   3/(10*h^(5/2)*(1+w)^(5/4))), tspan, h0);
graph4 = loglog(t,h,'--') % log-log plot, dashed line
set(graph4,'LineWidth',2)

% ODE for semi-dry foam, V_s = 5
[t,h] = ode45(@(t,h) -w^(-1/4)/(1/(5*h^(3/2)*(1+w)^(1/4))+
    3/(10*h^(5/2)*(1+w)^(5/4))), tspan, h0);
graph5 = loglog(t,h,'--') % log-log plot, dashed line
set(graph5,'LineWidth',2)
```

```
title('\textbf{Semi-dry foam: Log-log plot of $\tilde{h}$
    under all regimes}','Interpreter', 'latex','fontsize'
    ,16)
xlabel('Time ($\tilde{t}$)', 'Interpreter', 'latex', '
    fontweight','bold','fontsize',16);
ylabel('Lamella thickness ($\tilde{h}$)', 'Interpreter', '
    latex','fontweight','bold','fontsize',16);
legend({'$V_s \ll 1$', '$V_s \sim O(\epsilon^{-1})$', '$
    V_s = 0.3$', '$V_s = 1$', '$V_s = 5$'}, 'FontSize',16,'
    Interpreter', 'latex')

hold off
```

Listing B.6: Code for Figure 6.3

```
tspan = [0 1000]; % the range of t over which we will
    solve the ODEs
w = tan(pi/6) - pi/6 % defining our omega
h0 = 1/(1+w); % setting the initial condition for the ODEs

% ODE for dry foam, no surface viscosity
[t,h] = ode45(@(t,h) -h^(3/2)*(1-h)^(-1/4), tspan, h0);
graph1 = loglog(t,h) % log-log plot, solid line
set(graph1,'LineWidth',2)
hold on

% ODE for dry foam, medium surface viscosity
[t,h] = ode45(@(t,h) -10/3*(1+w)*h^(5/2)*(1-h)^(-1/4),
    tspan, h0);
graph2 = loglog(t,h) % log-log plot, solid line
set(graph2,'LineWidth',2)

% ODE for dry foam, V_s = 0.3
[t,h] = ode45(@(t,h) -(1-h)^(-1/4)/(1/(0.3*h^(3/2))+3/(10*
    h^(5/2)*(1+w))), tspan, h0);
graph3 = loglog(t,h,'--') % log-log plot, dashed line
set(graph3,'LineWidth',2)

% ODE for dry foam, V_s = 1
[t,h] = ode45(@(t,h) -(1-h)^(-1/4)/(1/(h^(3/2))+3/(10*h
    ^(5/2)*(1+w))), tspan, h0);
graph4 = loglog(t,h,'--') % log-log plot, dashed line
set(graph4,'LineWidth',2)

% ODE for dry foam, V_s = 5
```

```
[t,h] = ode45(@(t,h) -(1-h)^(-1/4)/(1/(5*h^(3/2))+3/(10*h
   ^(5/2)*(1+w))), tspan, h0);
graph5 = loglog(t,h,'--') % log-log plot, dashed line
set(graph5,'LineWidth',2)

title('\textbf{Dry foam: Log-log plot of $\tilde{h}$ under
    all regimes}','Interpreter', 'latex','fontsize',16)
xlabel('Time ($\tilde{t}$)', 'Interpreter', 'latex', '
   fontweight','bold','fontsize',16);
ylabel('Lamella thickness ($\tilde{h}$)', 'Interpreter', '
   latex','fontweight','bold','fontsize',16);
legend({'$V_s \ll 1$', '$V_s \sim O(\epsilon^{-1})$', '$
   V_s = 0.3$', '$V_s = 1$', '$V_s = 5$'}, 'FontSize',16,'
   Interpreter', 'latex')

hold off
```

Bibliography

[1] Anderson, A. M., Brush, L. N., and Davis, S. H. Foam mechanics: spontaneous rupture of thinning liquid films with plateau borders. *Journal of Fluid Mechanics 658* (2010), 63–88.

[2] Bailey, W. N. Generalized hypergeometric series.

[3] Barigou, M., and Davidson, J. Soap film drainage: theory of experiment. *Chemical Engineering Science 49(11)* (1994), 1807–1819.

[4] Bikerman, J. J. *Foams: Theory and Industrial Applications*. Springer, 1973.

[5] Breward, C. J. W. *The mathematics of foam*. PhD thesis, St. Anne's College, University of Oxford.

[6] Breward, C. J. W., Darton, R. C., Howell, P. D., and Ockendon, J. R. Modelling foam drainage. *I Chem E Symposium Series 142* (1997), 1009–1019.

[7] Breward, C. J. W., and Howell, P. D. The drainage of a foam lamella. *Journal of Fluid Mechanics 258* (2002), 379–406.

[8] Brush, L. N., and Davis, S. H. A new law of thinning in foam dynamics. *Journal of Fluid Mechanics 534* (2005), 227–236.

[9] Brush, L. N., and Roper, S. M. The thinning of lamellae in surfactant-free foams with non-newtonian liquid phase. *Journal of Fluid Mechanics 616* (2008), 235–262.

[10] Dewynne, J., Ockendon, J. R., and Wilmott, P. W. On a mathematical model for fibre tapering. *SIAM Journal on Applied Mathematics 49(4)* (1989), 983–990.

[11] Dey, D., Boulton-Stone, J. M., Emery, A. N., and Blake, J. R. Experimental comparisons with a numerical model of surfactant effects on the burst of a single bubble. *Chemical Engineering Science 52(16)* (1997), 2769–2783.

[12] Erneux, T., and Davis, S. H. Nonlinear rupture of free films. *Physics of Fluids A 5* (1993), 1117–1122.

[13] Howell, P. D. *Extensional Thin Layer Flows*. PhD thesis, St. Catherine's College, University of Oxford, 1994.

[14] Howell, P. D. The draining of a two-dimensional bubble. *Journal of Engineering Mathematics 35* (1999), 251–272.

[15] Mysels, K. J., and Cox, M. C. An experimental test of frankel's law of film thickness. *Journal of Colloid Science 17* (1962), 136–145.

[16] Ockendon, H., and Ockendon, J. R. *Viscous Flow*. Cambridge University Press, 1995.

[17] Ockendon, J. R., Howison, S. D., Lacey, A. A., and Movchan, A. B. *Applied Partial Differential Equations*. Oxford University Press, 2003.

[18] Ruckenstein, E., and K., J. R. Spontaneous rupture of thin liquid films. *Journal of the Chemical Society, Faraday Transaction 2: Molecular and Chemical Physics 0* (1974), 132–147.

[19] Schick, C. *A Mathematical Analysis of Foam Films*. PhD thesis, University of Kaiserslautern, 2004.

[20] Schwartz, L. W., and Princen, H. M. A theory of extensional viscosity for flowing foams and concentrated emulsions. *Journal of Colloid and Interface Science 118* (1987), 201–211.

[21] Taylor, J. E. The structure of singularities in soap-bubble-like and soap-film-like minimal surfaces. *Annals of Mathematics 103* (1976), 489–539.

[22] Verbist, G., Weaire, D. L., and Kraynik, A. M. The foam drainage equation. *Journal of Physics: Condensed Matter 8* (1996), 3715–3731.

[23] Weaire, D. L., and Hutzler, S. *The Physics of Foams*. Clarendon Press, 2001.